remote sensing

MDPI

Article

Landslide Susceptibility Mapping by Comparing GIS-Based Bivariate Methods: A Focus on the Geomorphological Implication of the Statistical Results

Laura Coco *, Debora Macrini, Tommaso Piacentini and Marcello Buccolini

Department of Engineering and Geology, Università degli Studi "G. d'Annunzio" Chieti-Pescara, 66100 Chieti, Italy; debora.macrini@alumni.unich.it (D.M.); tommaso.piacentini@unich.it (T.P.); buccolini@unich.it (M.B.)

* Correspondence: laura.coco@unich.it

Abstract: Landslide susceptibility is one of the main topics of geomorphological risk studies. Unfortunately, many of these studies applied an exclusively statistical approach with little coherence with the geomorphodynamic models, resulting in susceptibility maps that are difficult to read. Even if many different models have been developed, those based on statistical techniques applied to slope units (SUs) are among the most promising. SU segmentation divides terrain into homogenous domains and approximates the morphodynamic response of the slope to landslides. This paper presents a landslide susceptibility (LS) analysis at the catchment scale for a key area based on the comparison of two GIS-based bivariate statistical methods using the landslide index (LI) approach. A new simple and reproducible method for delineating SUs is defined with an original GIS-based terrain segmentation based on hydrography. For the first time, the morphometric slope index (MSI) was tested as a predisposing factor for landslides. Beyond the purely statistic values, the susceptibility maps obtained have strong geomorphological significance and highlight the areas with the greatest propensity to landslides. We demonstrate the efficiency of the SU segmentation method and the potential of the proposed statistical methods to perform landslide susceptibility mapping (LSM).

Keywords: landslide susceptibility; GIS; geo-statistics; landslide hazard; conditioning factors selection; DEM; geomorphometry; slope units; landslide susceptibility index; ROC curves

Citation: Coco, L.; Macrini, D.; Piacentini, T.; Buccolini, M. Landslide Susceptibility Mapping by Comparing GIS-Based Bivariate Methods: A Focus on the Geomorphological Implication of the Statistical Results. *Remote Sens.* **2021**, *13*, 4280. https://doi.org/10.3390/rs13214280

Academic Editors: Federica Bardi, Pierluigi Confuorto, Giulia Dotta, Diego Di Martire and Qingkai Meng

Received: 20 July 2021
Accepted: 18 October 2021
Published: 25 October 2021

1. Introduction

Landslide susceptibility (LS) can be defined as the probability that a landslide will occur in a given area based on terrain conditions without any temporal consideration [1]. It follows the principle that future slope failures are more likely to occur under the same conditions that have triggered past and present slope failures [2]. Certain terrain conditions can be considered as predisposing factors for the development of landslides. Triggering factors are temporary conditions that can directly cause landslides (e.g., earthquakes, rapid snow melt, and heavy rain). Landslide susceptibility maps are produced by considering conditioning factors only, whereas landslide hazard maps consider both predisposing and triggering factors [2].

Many models for landslide susceptibility mapping (LSM) have been developed using different methods, scales, and evaluation criteria [3], from knowledge-driven to process- and statistical-based models [4]. The most common and effective approaches in terms of the readability and usability of the output maps are based on more or less complex mathematical and statistical techniques, including (amongst others) logistic regression, neural network analysis, data overlay, index-based, and weight of evidence analyses, as well as machine learning (see [3] for a complete and up-to-date review). They require the a priori definition of the landslide inventory and predisposing factors and a rigorous procedure to calibrate and validate the models [5,6]. However, the complexity of the

elaboration methodology often prevents or at least makes their reproduction and application to different areas difficult. The most used mapping unit for LSM is the grid [3], which is in a matrix form, can be easily obtained in GIS, and is simple to handle for data processing. However, grid cells are not associated with geological–geomorphological environments, as they cannot represent the physiographic conditions of terrain. A more representative segmentation method comprises the unique condition units (UCUs) [7], which are homogenous domains with morphodynamically constrained spatial limits [8]. They maximize the internal homogeneity and the external heterogeneity of the selected parameters and therefore better approximate the morphodynamic response of the slope to the occurrence of landslides [9]. A particularly powerful segmentation method is based on geomorphological features, such as slope units (SUs), which are obtained by splitting the two halves of subcatchments and considering the slope gradient and aspect [10]. Some studies have demonstrated the efficiency of this kind of terrain segmentation, which can even outperform grid-based models [11–13]. One of the main strengths of SU segmentation is that the obtained landslide susceptibility maps are more readable and directly linked to the terrain structure [14].

The topic of landslide susceptibility has been the object of numerous scientific studies, many of which have an exclusively statistical approach focused on comparing a number of different techniques on the same dataset without a discussion of the meaning of the predictive relationships or of their coherence with morphodynamic models. It is necessary to translate the models into forecast maps that are useful for administrators as an effective tool for risk management.

The aim of this study was to obtain a landslide susceptibility map at the catchment scale for a key area (populated, with active slope failures), based on simple statistical methods and SUs segmentation, characterized by a strong geomorphological significance. The entire elaboration procedure was based on a multidisciplinary approach in which LiDAR-derived digital terrain model (DTM) analysis, digital orthophoto interpretation, and GIS processing were combined with direct field surveys and past geomorphological map analysis.

We constructed a new simple and reproducible method for delineating SUs with an original GIS-based terrain segmentation method based on hydrographic features. The SUs were chosen to be large enough to contain the entire alimentation area of a landslide or a portion of that but small enough to be the reference slope area of a single landform.

We performed LS analysis by comparing two GIS-based statistical methods. We chose to apply bivariate statistical methods based on the landslide index approach [15], originally developed for grid-cell analysis, by adapting the equations. These two methods are simple and intuitive, and the advantage of using bivariate statistics is that they immediately reveal the relation of the predisposing variables with the propensity for landslides.

We selected the Piomba Stream basin, in Central Italy, as the test area. This is a strongly anthropized area, and the hillslopes are particularly prone to slope failures due to the geomorphological and geological features. This area has been studied for many years as an important site for the interaction of both human pressure and slope morphometry on erosion processes (e.g., [16–19]). Recent studies have focused on the role of precipitation on landslides in this area and evidenced that rainfall is the main triggering factor [20,21]. However, no studies have applied LS modeling.

The predisposing factors were selected after an intense and prolonged field survey in order to choose the most effective factors based on field evidence, picking the parameters most commonly used in the literature for evaluating LS [22,23]. We considered only one parameter for each terrain characteristic, avoiding redundancies, which could have generate overlapping effects and interrelationships that are difficult to discriminate [3]. Moreover, we tested the use of the morphometric slope index (MSI) [24] as a predisposing morphometric factor for landslides and the possibility of considering MSI as an alternative to the slope gradient and other slope morphometric variables. It is a single effective parameter for slope morphometry and is the result of the geomorphological dynamics, as it

highlights all those processes that have changed the morphological structure of the terrain over time. It reflects the history of the slope and its modeling.

The entire LS analysis was framed within an experimental design that combined statistical methods, predisposing factors, and the areal threshold of landslides. The main outcomes of this research demonstrate the efficiency of the SU segmentation method and the potential of the proposed statistical methods for determining the LSM, producing easy-to-read susceptibility maps. Beyond the purely statistical values, the proposed models adhere to the geomorphological significance of the terrain and highlight the areas with the greatest landslide propensity.

2. Materials and Methods

2.1. Study Area

The Piomba Stream is located in the hilly coastal area of the Central-Eastern Apennines (Abruzzo Region, Italy; Figure 1). This W–E-elongated basin flows from Mt. Giove (747 m a.s.l.) to the Adriatic Sea, near the town of Silvi (PE). The drainage pattern is mostly trellis-like and subordinately dendritic, with few small tributary channels. The main tributary is Fosso del Gallo in the hydrographic left side.

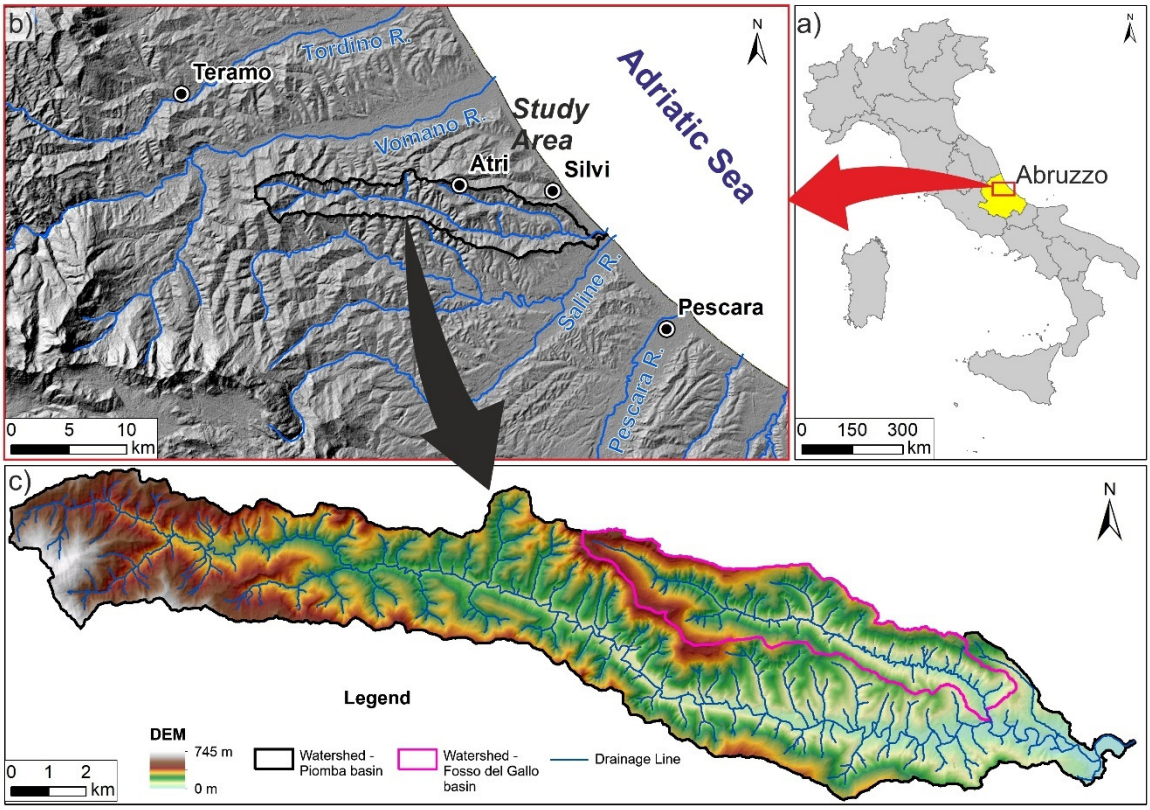

Figure 1. Geographical location of the study area in Italy (**a**) and northern Abruzzo (**b**); DTM of the Piomba and Fosso del Gallo basins (**c**).

The area is characterized by a Mediterranean climate with a sub-temperate littoral regime [25]. Mean annual temperatures are generally between 12.5 and 15.5 °C, and the mean annual rainfall is between 600 and 800 mm. Precipitation increases toward the mountains with a trend not proportional to the elevation. The maximum rainfall is in autumn, with a secondary maximum in spring. Summers are rather dry, especially near the coast and on the hills with lower elevation.

The study area belongs to the outermost eastern sector of the Apennine chain, which features a NE-verging thrust belt geometry, dissected by several younger normal faults. The piedmont areas are mainly affected by extensional basins to the west and buried thrusts

overlain by homocline plateau, mesa, and cuesta landscapes to the east [26]. The sediment outcrops are mainly foredeep siliciclastic sequences belonging to the Plio–Pleistocene succession, which become progressively younger moving toward the Adriatic Sea and are arranged according to a homocline slightly dipping towards the NE. They are mainly composed by clayey/sandy-clayey sediments, often interbedded with clastic deposits (sands and conglomerates with lenticular geometry, sometimes very thick) at various stratigraphic heights. In the areas near the coast, the hills' summits are covered by thick deposits of sands, gravels, and conglomerates of fluvial–deltaic and coastal environments [27,28]. At the highest elevations of the foothills, clayey marl and marly clay alternate at sandy and clayey levels. They belong to three main geological formations [29]: the Laga Formation (Messinian–Lower Pliocene p.p.), which includes the older and innermost turbiditic sequence (the westernmost part of the Piomba basin); the Cellino Formation (lower Pliocene), which includes a younger and more external foredeep turbiditic sequence (the central part of the Piomba basin); and the Mutignano Formation (upper Pliocene–lower Pleistocene), the post-orogenic sequence deposited within the Periadriatic Basin (the easternmost part of the Piomba basin) (Figure 2). The homoclinal valleys are engraved along the clayey levels with marked asymmetry. The rivers, which flow according to the regional topographical gradient from W to E, have a cuesta morphology [17].

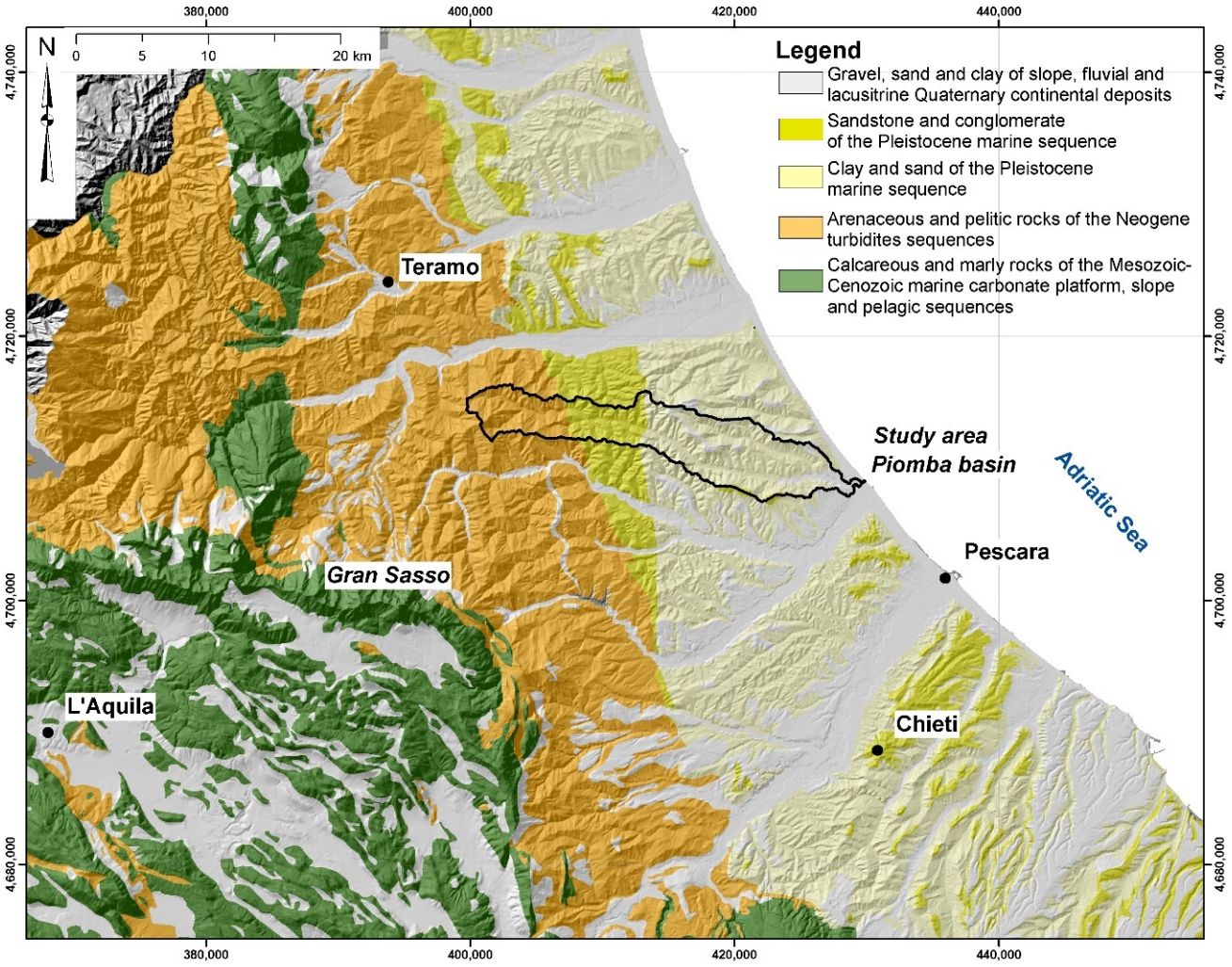

Figure 2. Geologic scheme of the Abruzzo region. The black line indicates the watershed boundary of the study basin (grid in UTM WGS84 coordinates, UTM zone 33 N).

The geomorphological evolution of the area was strongly influenced by the outcropping lithology, the tectonic structure, and the regional uplift, and by climatic- and sea-level changes [27]. This produced the relative sea-level changes and local base level changes (negative in the long term in comparison to today's sea level). The present landscape was shaped by the Pleistocene–Holocene geomorphological dynamics. During the Pleistocene, the rapid uplift and the alternation in climatic phases produced the deepening of the hydrographic systems and the dismantling of the summit conglomerate, which led to the outcrop of the clayey substrate [26]. Fluvial and slope processes were recorded in a complex sequence of continental deposits (post-orogenic) overlying the bedrock [30]. In the Holocene, fluvial, gravitational, and anthropic processes allowed the landscape to be shaped especially through mass movements (slides, flows, and falls), badlands, gully and rill erosion, slope remodeling, and de- and reforestation due to agricultural practices [16,17,19,20]. The mass movements and landslides are mostly active and recent, and the main triggering factor is high precipitation, the effect of which has combined with the general drainage dissection, terrain morphology (particularly slope gradient and concavity [21]), and land use [20].

2.2. Landslide Susceptibility Analysis

The data necessary to complete the landslide susceptibility analysis were obtained by means of a multidisciplinary approach that included geomorphological field survey, remote sensing (air photo analysis), DTM processing, and institutional open data. We used color aerial photos, regional topographic maps (*Carta Tecnica Regionale*, CTR, 2007) and DTMs provided by the Cartographic Office of the Abruzzo Region (Table 1) to derive the morphological and hydrological variables (i.e., the geometry of SUs, landslide inventory, land use, and drainage density). This improved the feasibility and repeatability of the analysis and will lead to future improvements with multitemporal analysis for the investigation of the trends in landslide susceptibility. The aerial photos were obtained with LiDAR flights, which were orthorectified and georeferenced with a pixel resolution of 0.2 m. The CTRs were produced using photogrammetrical techniques from the digital orthophotos at a 1:10,000 scale. The DTMs were LiDAR-based with a 10 m cell-size resolution. The geological and geomorphological variables were obtained through the field survey with the support of the Hydrogeological Setting Plan of Abruzzo Region (Piano per l'Assetto Idrogeologico, PAI) [31] and the Italian Landslides Inventory (Inventario dei Fenomeni Franosi in Italia, IFFI) [32] maps.

Table 1. Sources of input data.

Geodatabase Layers	Derived from	Scale	Data Source
Landslide inventory	Field survey	1:10,000	This paper
	Color aerial photos	1:10,000	Abruzzo Region (2009)
	PAI	1:25,000	Autorità di Bacino (2005)
	IFFI	1:25,000	ISPRA (2007)
Predisposing factors			
Bedrock lithology	Field survey	1:10,000	this paper
Land use/land cover	Corine Land Cover	1:10,000	CLC (2018)
Deposit thickness	DTM Borehole analysis	10 m cell-size	Abruzzo Region (2015)
Slope aspect	DTM	10 m cell-size	Abruzzo Region (2015)
Drainage density	DTM	10 m cell-size	Abruzzo Region (2015)
	CTR	1:10,000	Abruzzo Region (2007)
	Color aerial photos	1:10,000	Abruzzo Region (2009)
Slope gradient	DTM	10 m cell-size	Abruzzo Region (2015)
Morphometric slope index	DTM	10 m cell-size	Abruzzo Region (2015)

The input data were collected in a geodatabase built in the GIS environment and organized in two categories: landslide inventory and predisposing factors (Table 1). All the

parameter processing and morphometrical analyses were performed in ArcGIS (ArcMap® 10.1, ESRI, Redlands, CA, USA). The data analysis was performed via bivariate statistics by comparing the results of the two landslide indexes. The SUs were considered as mapping units of the LS models.

2.2.1. Landslide Inventory

The landslide inventory was compiled through an integrated approach combining field and remote investigations. In the preliminary phase, pre-compiled regional maps were analyzed: PAI [31] and IFFI [32]. Afterward, the remote observation from aerial photographs allowed us to map the surface distribution of the landforms with GIS software. Finally, all the landforms were observed and measured in the field for ground-truthing.

A detailed geomorphological field survey was performed between spring 2017 and autumn 2019. In particular, from January to April 2017, heavy rainfall activated numerous shallow mass movements that were investigated in the field survey. The final product was the Geomorphological Map of Torrente Piomba catchment at a 1:10,000 scale (resized in a schematic map in Figure 3), from which the landslide inventory map and some predisposing factors maps were derived. The landslide inventory includes active/dormant features, inventoried in the GIS-based geodatabase, which are classified according to the Varnes [33] classification of landslides.

2.2.2. Predisposing Factors

The predisposing factors for landslides were chosen in relation to the terrain morphometry, geology and geomorphology, hydrology, vegetation, and anthropic features. The selection was based on field evidence, expert knowledge of the study area, a methodological approach from previous studies, and local data availability [22,23,34]. Seven controlling factors were considered from those that showed the greatest influence on landslides: bedrock lithology (L), land use/land cover (LULC), deposits thickness (T), slope aspect (A), drainage density (D), slope gradient (S), and morphometric slope index (MSI). Each factor was subdivided into different classes that represent their entire variability, according to the accuracy and scale of the data source. For the categorical factors (L and LULC), the majority class within the SU was considered. The numerical factors (D, S, and MSI) were calculated from vector layers (polygons, polylines) applying the appropriate formula. The slope aspect (A) was derived from the DTM, and the median was calculated in order to consider the most prevalent value in each SU. The deposit thickness (T) was extrapolated from morphometric variables and then subdivided into qualitative classes. Afterward, A and T were considered categorical variables.

Bedrock lithology (L). The bedrock lithology was selected as it is recognized to be one of the most important factors in LSM because it influences the slope stability, the size and the type of landslides, and subsequently the susceptibility degree [35,36]. In our study, the bedrock lithology map was derived from the field-based geomorphological map. We followed a lithotechnical approach, moving from a lithological basis and grouping the geological units into four classes of rock types (Figure 4a): fluvial deposit, sandstone and conglomerate, clay, and alternating sand and clay. Each SU was assigned the prevailing class in terms of areal distribution.

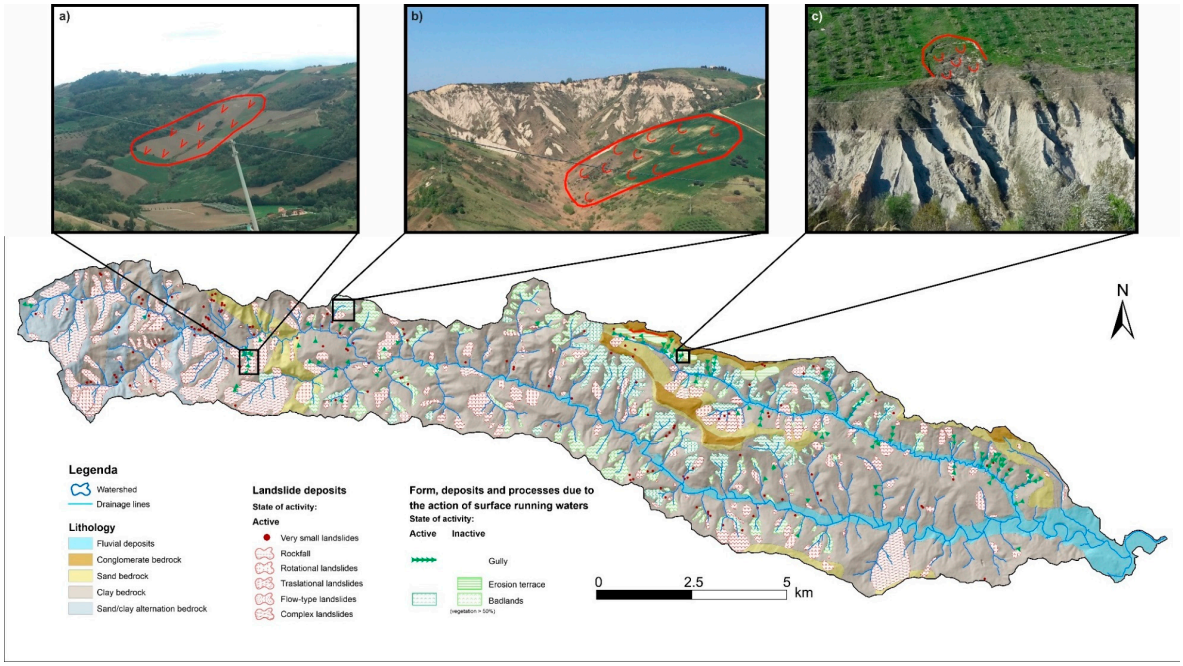

Figure 3. Schematic Geomorphological map of Torrente Piomba catchment derived from a 1:10,000 field survey with some representative landforms: (**a**) rotational landslide; (**b**) flow type landslide on the side slope of a badland basin; (**c**) a very small landslide at the top of a badland.

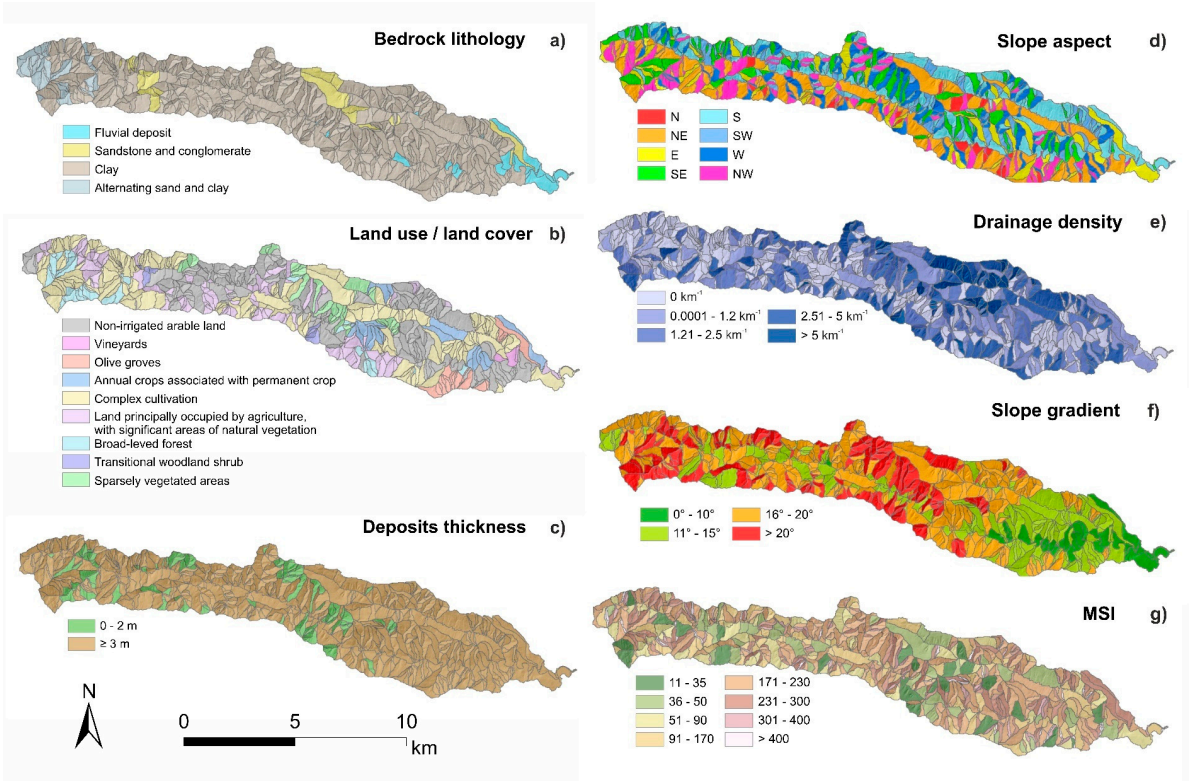

Figure 4. Schemes of the distribution of the landslide-predisposing factors in the studied basin: (**a**) bedrock lithology derived from field survey; (**b**) land use/land cover derived from the Corine Land Cover maps; (**c**) deposit thickness extrapolated by a linear relation from the slope; (**d**) slope aspect derived from the DEM; (**e**) drainage density derived from the Regional Topographic Maps of Abruzzo Region; (**f**) slope gradient derived from the average slope of the SU; (**g**) MSI calculated from a combination of morphometric features from the DEM.

Land use/land cover (LULC). The importance of LULC in slope stability is recognized in particular for areas subjected by a strong anthropic impact [16,37,38], such as the piedmont areas of Central Italy. The variability in vegetation cover can directly influence the soil infiltration capacity and consequently the slope stability [39]. Moreover, natural or artificial changes in LULC can weaken and destabilize the slopes. In our study, the LULC was derived from the Corine Land Cover project—Level 3 [40] and implemented through the analysis of orthorectified aerial photos. Nine types of LULC are relevant in the study area (Figure 4b): vineyards, olive groves, complex cultivation patterns, land principally occupied by agriculture with significant areas of natural vegetation, annual crops associated with permanent crops, broad-leaved forest, non-irrigated arable land, transitional woodland shrub, and sparsely vegetated areas.

Deposits' thickness (T). The thickness of superficial deposits (i.e., mainly continental colluvial and slope deposits in the study area) was selected as it is recognized to be one of the strongest factors influencing surface processes determining infiltration rates, overland flows, and water storage potential [41,42]. These thickness data were derived from direct observations (e.g., boreholes) or from indirect estimation. In the study area, direct observations were not available in sufficient amounts to derive an extensive deposit thickness map to be able to predict their depth with an accuracy compatible with the requirements of LSM [43]. The available data were concentrated into small, urbanized areas, and could not be extrapolated for the entire basin. In these cases, an indirect geostatistical analysis can be applied to estimate the thickness through DEM-derived morphometric variables [43,44]. Therefore, we extrapolated T by using the equation developed by Sciarra et al. [45] for an area with similar bio-geo-climatic conditions. This is a linear pixel-based relation that links T to the local slope (tan β):

$$D = -6.34 \tan \beta + 5.49. \quad (1)$$

The few data from direct measurements were used to check the values of T. The depths were validated by comparing the direct measurement data with the values of the estimation via the formula and making sure that the measured value was within the range of the estimated value. The most prevalent value of T was extracted in each SU as a median value via the zonal statistics. We divided T into two classes (Figure 4c) to discriminate between absent/very shallow and deep deposits ($\leq$2 m and >2 m, respectively).

Slope aspect (A). The role of the slope aspect in slope stability is debated since different studies have reported opposite outcomes ([46] and references therein). Some results suggested that A is an important predisposing factor for superficial landslides in clayey deposits and is correlated with other factors such as bedrock structure [46,47]. As already stated, we derived A from the DTM and calculated its median value in each SU using the Zonal Statistics tool. Then, we grouped the eight main directions with an angle step of 45° (N, NE, E, SE, S, SW, W, and NW) (Figure 4d).

Drainage density (D). The drainage density is a traditional hydrological parameter that was developed by Horton [48] and represents the degree of fluvial dissection. It is strictly influenced by the slope gradient and the lithology. We selected D because it influences the slope stability and highlights hydrological critical conditions or critical fluvial erosion [49–51]. D is expressed as the length of the drainage network per unit area and calculated as the ratio between the total stream length and the basin area. The value of D can be influenced by the mapping scale and strictly depends on the channel head's source area [50]. We derived the drainage network as a vector layer from the Regional Topographic Maps of the Abruzzo Region at a 1:5000 scale (CTR, 2007) at the same scale as the other predisposing factors and verified and implemented this through aerial photo analysis. The hydrographic layers are LiDAR-based and accurate enough with respect to the terrain morphometry. Then, we calculated D for each SU. This factor was classified into five classes using the natural break algorithm (Figure 4e), with each corresponding to a certain range of D values (in this case, the ranges are 0, 0.0001–1.2, 1.2–2.5, 2.5–5, and 5–9.7 km^{-1}).

Slope gradient (S). The slope gradient is the main morphometric variable that affects the slope stability at different scales (e.g. [3,52,53], amongst many others). It controls not only slope-gravity-induced processes but also hydrological processes, runoff, soil erosion, weathering, vegetation cover, and human activities, which in turn influence slope stability. We calculated S using the Add Surface Information tool, which attributed the average percentage of the slope to each SU and then transformed it into degrees. This factor was divided into four classes (0°–10°, 11°–15°, 16°–20°, and >20°; Figure 4f).

Morphometric Slope Index (MSI). The morphometric slope index (MSI) was recently introduced as a unique reference index to study the influence of pre-incision slope morphometry on the evolution of drainage networks and mass movements within Italian badlands and small clayey basins [19,24,54,55]. It groups the main (linear and areal) morphometric features of a morphological unit with the formula:

$$MSI = L \cdot R_C \cdot A_{3D}/A_{2D} \quad (2)$$

where L is the length, R_C is the circularity ratio, A_{3D} is the three-dimensional surface area, and A_{2D} is the plane surface area. In this study, we used MSI to characterize all morphometric features of the SUs and provide a more complete alternative to the use of S. It considers the slope's gradient (expressed through the relationship between the 3D and 2D area), shape, and size (length and width). The single parameters were calculated as vector (polygon) characteristics via specific tools in ArcGIS (Minimum Bounding Geometry for L, Interpolate Shape/Add Surface Information for A_{3D}, Calculate Geometry for A_{2D}, and the perimeter p used for $R_C = 4\pi A_{2D}/p^2$). MSI was subdivided into eight classes (Figure 4g) by modifying the natural break algorithm ranges (11–35, 35–50, 50–90, 90–170, 170–230, 230–300, 300–400, and >400 m).

2.2.3. Mapping Units

In this study, we used the SUs as mapping units to assess landslide susceptibility. The SUs were derived using the Arc Hydro toolbox in ArcGIS, with little or no handling by the operator.

As a base layer, the LiDAR-based DTM with a 10 m resolution was used from the Abruzzo Region geodatabase (Figure 1). The step-by-step procedure to delineate the SUs is shown in Figure 5. The first phase was the terrain preprocessing, in which the DTM was corrected to clearly identify the drainage cells. The second phase was the terrain processing, in which the sub-basins were delineated and then divided into two by the main streams, in order to obtain the two halves of the catchment. To carry out this operation, the main drainage lines were extended until they intersected the watershed divides using the Longest Flow Path for Catchments tool. Subsequently, this longest flow path was used to cut the hydrographic unit into two SUs. Then, the aspect was derived via its median value in each SU using the Zonal Statistics tool. Using an iterative procedure, the smaller areas were aggregated to the larger adjacent ones, and the neighboring units in the same aspect range were joined. In this way, only the SUs greater than 10,000 m^2 with a uniform aspect were maintained.

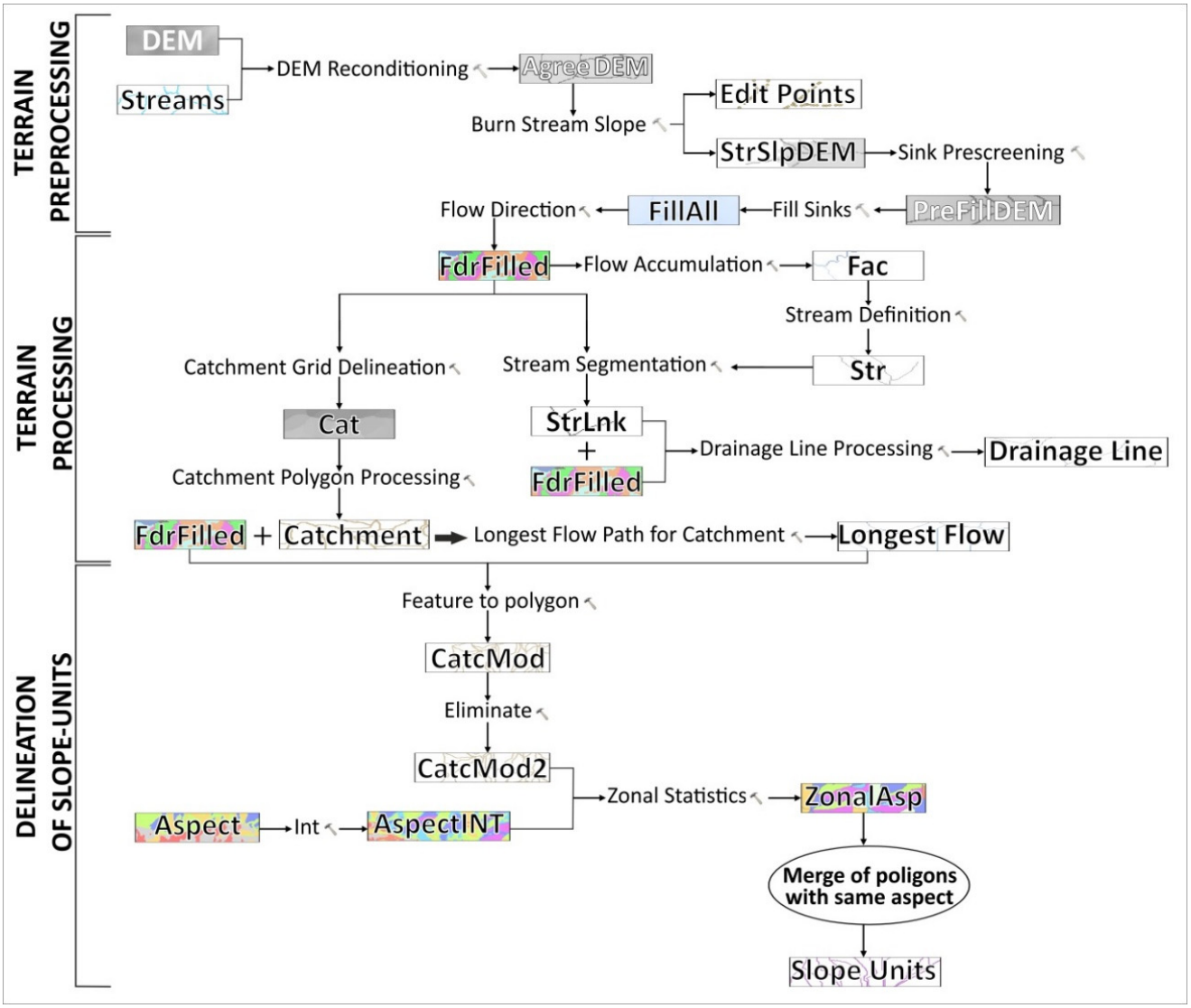

Figure 5. Workflow of the step-by-step procedure to delineate the SUs.

2.2.4. Landslide Susceptibility Methods

To perform the LSM of the study basin, we chose to test two GIS-based bivariate statistical methods and to compare their results to establish which is the most powerful method for predicting landslides. The first is the landslide susceptibility index (LSI) developed by Romeo et al. [56] according to Lee and Min [57]; the second is a simplified version of LSI named the landslide index (LI) developed by Sciarra et al. [45]. The advantage of these methods is to provide an immediate measure of the role played by each factor and related classes on landslide susceptibility [56]. Both methods were designed to work on raster data and have been modified and adapted so that they can also be used on vector data. They measure a percentage-weighed sum of the predisposing factors ranging from 0 (least influence) to 100 (most influence). The complete workflow of the statistical analysis is shown in Figure 6.

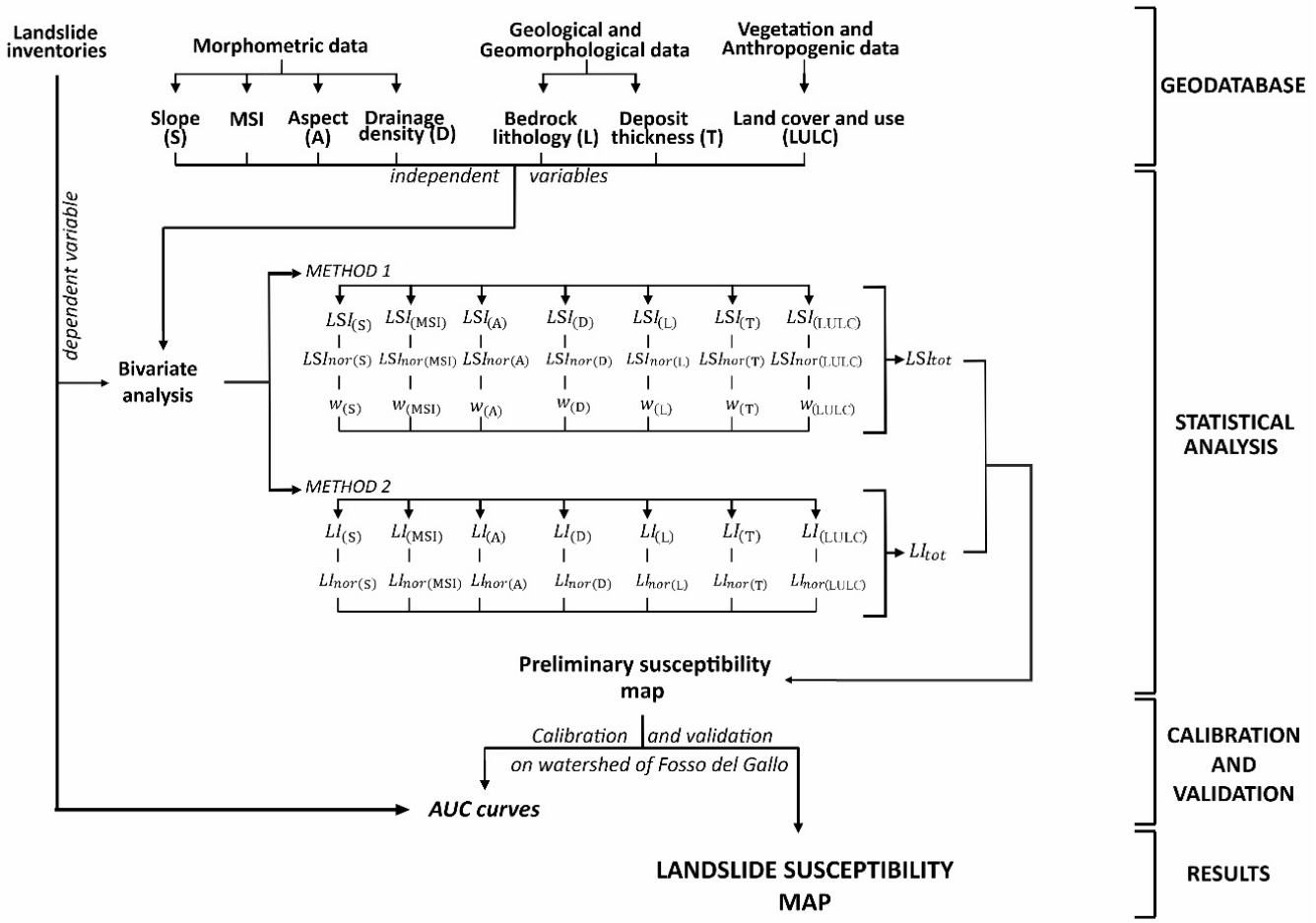

Figure 6. Workflow of the statistical analysis.

Landslide Susceptibility Index (LSI)

Originally, the LSI was created for raster-based LSM and was calculated by summing the ratio between the number of cells in which landslides occur and the number of cells in which landslides did not occur for each class of a factor. We transformed this calculation for the SU-based LSM into the ratio between the landslide area and the non-landslide area in the SUs for each class of a factor.

LSI is defined as the ratio between a and b, expressed in the following equation:

$$\begin{gathered} LSI_i = a/b, \\ a = A(f_i)/A\ (F), \\ b = A(s_i)/A(S). \end{gathered} \tag{3}$$

The parameter a is the ratio between the landslide surface of each class ($A(f_i)$) and the total landslide surface in the study area (A (F)), while parameter b is the ratio between the non-landslide area of each class ($A(s_i)$) and the total non-landslide area in the study area (A(S)). LSI was calculated for all the classes of each factor and then normalized to compare the data:

$$LSI_{nor,i} = LSI_i/LSI_{i(max)} \times 100. \tag{4}$$

where LSInor represents the value of LSI for each class (i) of a factor divided by the maximum LSI value in the same factor and multiplied by 100. It quantifies the impact of the classes taken individually.

The total LSI was obtained from the combination of the LSInor for each SU:

$$\begin{aligned} LSI_{tot} &= \sum (LSI_{nor,i} \times w_j) \\ w_j &= LSI_{nor,i(min)} / \sum LSI_{nor,i(min)}. \end{aligned} \quad (5)$$

LSItot is given by the sum of the LSInor of each factor multiplied by the weight of the factor (wj). The weight of a factor is expressed as the ratio between the value of the minimum LSInor of the classes and the sum of the minimum LSInor of all the factors. LSItot expresses the propensity for failure due to the weighted combination of the considered predisposing factors.

LSItot was assigned to each SU and the corresponding values w3re classified according to the Jenks' method (natural breaks). Five susceptibility classes were created: very high, high, moderate, low, and very low.

Landslide Index (LI)

The LI was created to work in raster-based LSM, in the same manner as LSI. In this case, however, we applied the equation to the SU-based LSM as it is because LI is calculated as the ratio between the landslide area of each class (i) and the total surface of the class:

$$LI_i = A(f_i)/A_i. \quad (6)$$

The values obtained for the classes of each factor were normalized to 100:

$$LInor,i = LIi/LIi(max) \times 100 \quad (7)$$

where LI_i represents the value of the LI for each class, which is divided by the maximum LI value within the same factor and multiplied by 100. The total landslide index was obtained by the sum of the LI_{nor} of each factor divided by the total number of factors (N):

$$LItot = \sum LI(nor,i)/N \quad (8)$$

This expresses the propensity for instability due to the mathematical combination of predisposing factors. Furthermore, in this case, the SUs were classified and mapped according to the natural breaks method into five levels of susceptibility: very high, high, moderate, low, and very low.

2.2.5. Training and Validation

The training and validation phases were performed using the success rate and prediction rate curves to test the model accuracy and prediction skills.

For the training phase, the whole area of the basin of the T. Piomba without the basin of the Fosso del Gallo was considered as the test area (Figure 1), from which the susceptibility model was developed to determine the performance of the model. The calibration of the models was constructing by creating the ROC curves as plot charts, in which the cumulative percentage of the SU area for each susceptibility level is reported on the x-axis and the cumulative percentage of landslide areas for each susceptibility level is reported on the y-axis. To evaluate the reliability of the statistical method, the area under the curve (AUC) was calculated. The AUC can range between 0 (invalid) and 1 (high reliability). Generally, the model is considered valid if AUC $\geq$ 0.7 [58]. The calculation of AUC allows us to compare different models.

For the validation phase, the Fosso del Gallo sub-basin was chosen as the validation area (Figure 1). This allowed us to evaluate whether the models can work even in areas other than those in which it was created and thus to test its capacity to predict future landslides. Once the model was obtained, it was applied to the validation area according to the same susceptibility levels, and its predictive performance was measured through the calculation of the AUC of the ROC curves.

2.2.6. Experimental Design

The research was organized in a 2 × 3 × 2 experimental design (Table 2) combining the statistical methods (2×), the combination of predisposing factors (3×), and the areal threshold of landslides (2×). Both statistical methods, LSI and LI (2×), were applied with different combinations of factors (3×), where one considered all the seven factors and the other two considered only one morphometric factor (alternatively S or MSI) together with the other six. This was carried out to test the hypothesis that MSI alone is sufficient to describe the morphometric characteristics of the SU, without the need to consider other factors, such as S. Furthermore, for each application, two models (2×) were employed according to the areal threshold of landslides: one considering all the mapped landslides and the other considering the SUs with less than 2% of the area covered by landslides as free of landslides [59]. A total of 12 landslide susceptibility maps were generated and then compared through the training and validation procedure to establish which achieved the best performance in terms of reliability and prediction skills.

Table 2. Scheme of the experimental design of the study.

		Statistical Methods					
		LSI			**LI**		
Areal Threshold	*no*	**LSI_1 w1**	**LSI_3 w3**	**LSI_5 w5**	**LI_7**	**LI_9**	**LI_11**
	>2%	**LSI_2 w2**	**LSI_4 w4**	**LSI_6 w6**	**LI_8**	**LI_10**	**LI_12**
		L, LULC, T, D, A, S, MSI	**L, LULC, T, D, A, S**	**L, LULC, T, D, A, MSI**	**L, LULC, T, D, A, S, MSI**	**L, LULC, T, D, A, S**	**L, LULC, T, D, A, MSI**
		Factor combination					

3. Results

3.1. Landslides

In the landslide inventory map (Figure 7), a total of 265 landslides were reported, covering an area of 15.5 km^2, corresponding to 14.8% of the basin (105 km^2). Many of the landslides occurred on cultivated sites, and their morphological evidence was modified or removed by farming practices. Therefore, the pre-existing PAI and IFFI inventories allowed us to identify the correct location of some of the mapped landforms whose boundaries were correctly traced during the field activity and the air-photo analysis. In addition, more recent landslides were mapped during the field activity and the air-photo analysis. As observed after the rainfall events, the main triggers of mass wasting in the study area were heavy rainfalls, which caused the activation or the reactivation of most of the landslides.

The majority of the landslides were of the flow type (223 out of 265). In the areas in which they occurred, the substrate was mainly clayey, favoring their (re-)activation in the rainy periods due to water infiltration. There were 24 rotational landslides, leading to a number of counterslopes mostly set at the foot of the concave sliding surfaces. All the 16 complex landslides had a rotational component, and most of them were located near the source area of T. Piomba. A single landslide with a translational component was located on the right bank of the Fosso del Gallo. There was also a rockfall on the left bank of the Fosso del Gallo below the town of Atri, involving the summit conglomerates.

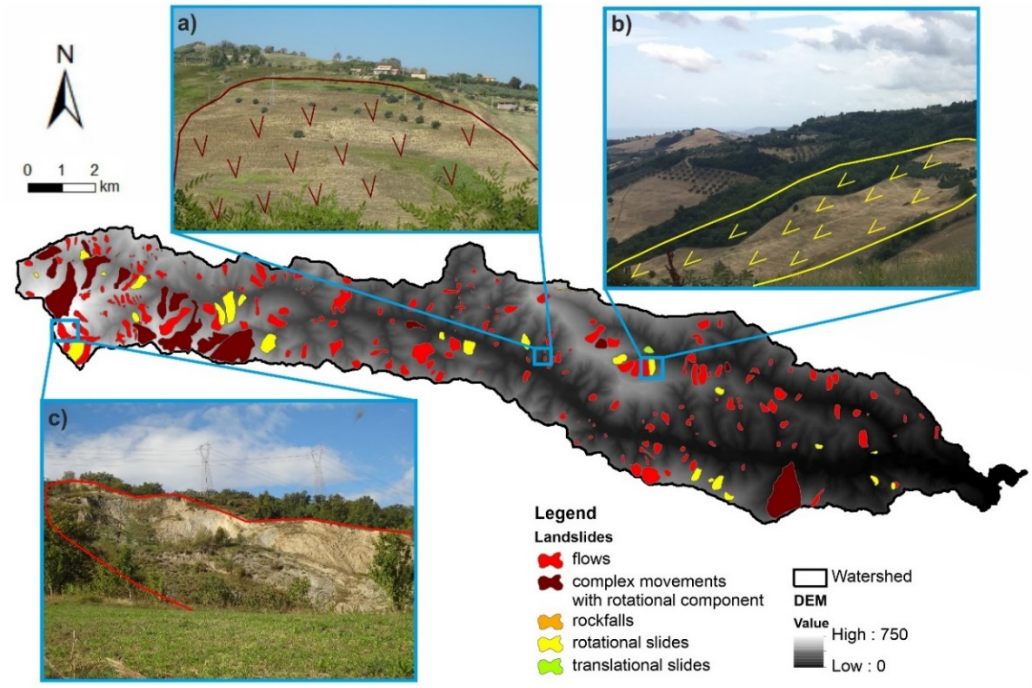

Figure 7. Landslide inventory map with some details of the most representative landslides: (**a**) complex landslide with rotational component (#162); (**b**) rotational landslide (#251); (**c**) flow-type landslide (#26).

3.2. Characterization of the SUs

The T. Piomba basin was divided into 613 Sus (Figure 8): 518 in the test area and 95 in the validation area. In the test area, the smallest SU was 0.012 km^2, the largest was 1.05 km^2 (mean = 0.17 km^2, median = 0.118 km^2), and most of the SUs were between 0.012 and 0.4 km^2 (96.3%). In the validation area, the smallest SU was 0.015 km^2, the largest was 1.8 km^2 (mean = 0.2 km^2, median = 0.117 km^2), and most of the SUs were between 0.015 and 0.4 km^2 (91.6%). This suggests that SU sizes were comparable in the test and validation areas.

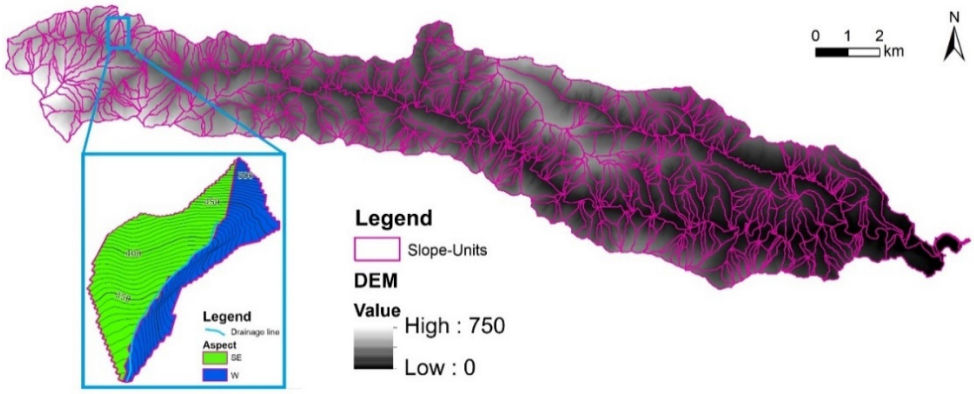

Figure 8. Subdivision of the basin in SUs with a detail of the segmentation process (in the inset, contour equidistance of 10 m).

In test area, the number of SUs with landslides amounted to 259; while considering an areal threshold of 2% of landslides, the total was 251. In the validation area, the number of SUs with landslides amounted to 40; while considering the areal threshold of 2% of landslides, the total was 37. Each SU was assigned a class of factors.

3.3. Landslide Susceptibility Models

The LSI and LI statistical methods were applied to the six different situations of the experimental design combining areal threshold and predisposing factors (Table 2). A total of 12 susceptibility maps were obtained: 6 maps for each statistical method. The models were coded by adding a consecutive number as a suffix to LSI and LI. The susceptibility maps were arranged into five classes, and LSI_{tot} values were divided by means of natural breaks each time (Figures 9 and 10, Tables A7 and A8).

3.3.1. LSI Models

The LSI bivariate statistics described the influence of the classes of each factor (Tables A1 and A3). Most of the landslides developed in SUs with alternating sand and clay bedrock and broad-leaved forests (and subordinately olive groves), with a high deposit thickness (>2 m), northern aspect (primarily NW, and subordinately N and NE), low D (primarily 0.0001–1.2 km^{-1}, and in general below 5 km^{-1}), medium-high slope gradient (16–20°, and in general above 11°), and high MSI (>400 m). This is valid if we consider the areal threshold of 2% for the landslide surface.

The weighted equation for LSI_{tot} was different for each case because the weights of the factors (Tables A2 and A4) assume different values according to the influence of the factor. In any case, the models produced similar results in terms of the relative importance of the factors. D, MSI, and T were the most influential factors; A and S were moderately influential; and L and LULC were the least influential. Comparing the models that considered both MSI and S (LSI_1 and LSI_2), MSI was always found to be the most influential morphometric variable. In the cases in which MSI was not included in the analysis (LSI_5 and LSI_6), the influence of S was found to be secondary. In the cases where S was not included in the analysis (LSI_3 and LSI_4), the influence of MSI was even higher.

In general, the susceptibility maps (Figure 9, Table A7) show that the SUs with very high and high susceptibility were mainly located on the right hydrographic side of the T. Piomba. The SUs with moderate susceptibility were located on the left side. The SUs with low and very low susceptibility were mainly located on the left side and in the areas close to the mouth.

3.3.2. LI Models

The LI bivariate statistics describe the influence of the factor classes and not the relative importance of the factors because the equation for LI_{tot} depends on the number of factors, assuming that they have the same weight (Tables A5 and A6). The relative influence of the classes is similar to the LSI models, as well as the distribution of the susceptibility in the SUs. There were only small differences among the models concerning the absolute values of the indices and not their relative relationship. The most influential factor classes were alternating sand and clay bedrock and broad-leaved forests (and subordinately olive groves) with a high deposit thickness, a NW aspect (and subordinately N and NE), low D (<5 km^{-1}), medium-high slope gradient (>11°), and high MSI (>400 m). Very-high- and high-susceptibility SUs were mainly located on the right hydrographic side of the T. Piomba, while moderate susceptibility SUs were on the left side, and low and very low susceptibility SUs were on the left side and close to the mouth (Figure 10, Table A8).

3.3.3. Training and Validation

The training and validation procedure was performed via the ROC curves (Figure 11), as already described. The AUC values of the LSI models were between 0.65 and 0.67. Therefore, the model training accuracies were between 65% and 67%. The AUC values of the validation set were between 0.66 and 0.69, reaching a prediction accuracy between 66% and 69%. Not one of the LSI models reached the minimum threshold of the AUC value for reliability, with values slightly below 0.7 [58]. The LSI model with the highest AUC values was LSI_1, which considered all the parameters and all the landslides without the areal threshold of landslides.

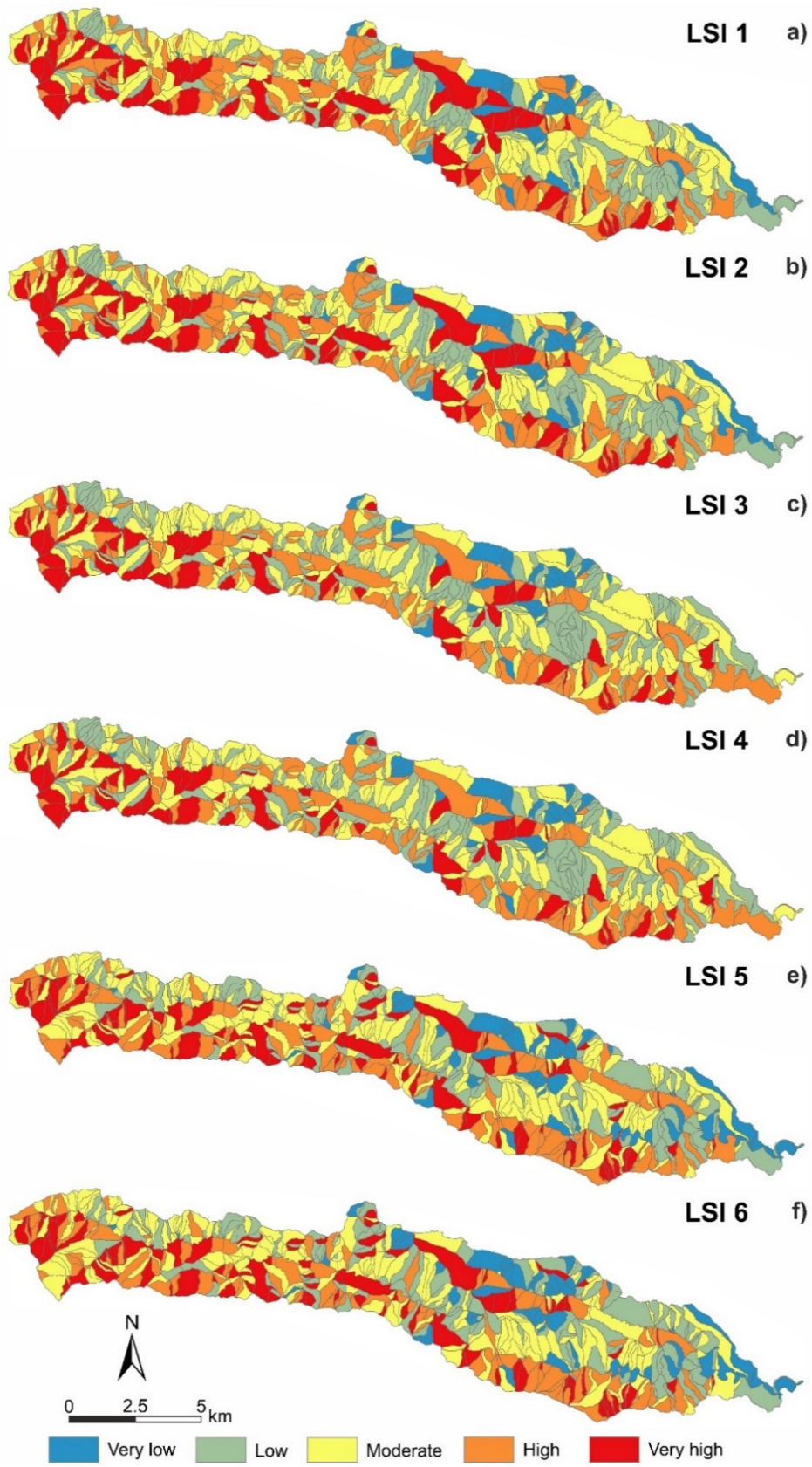

Figure 9. Landslide susceptibility maps created with the LSI method: (**a**) LSI_1 model; (**b**) LSI_2 model; (**c**) LSI_3 model; (**d**) LSI_4 model; (**e**) LSI_5 model; (**f**) LSI_6 model.

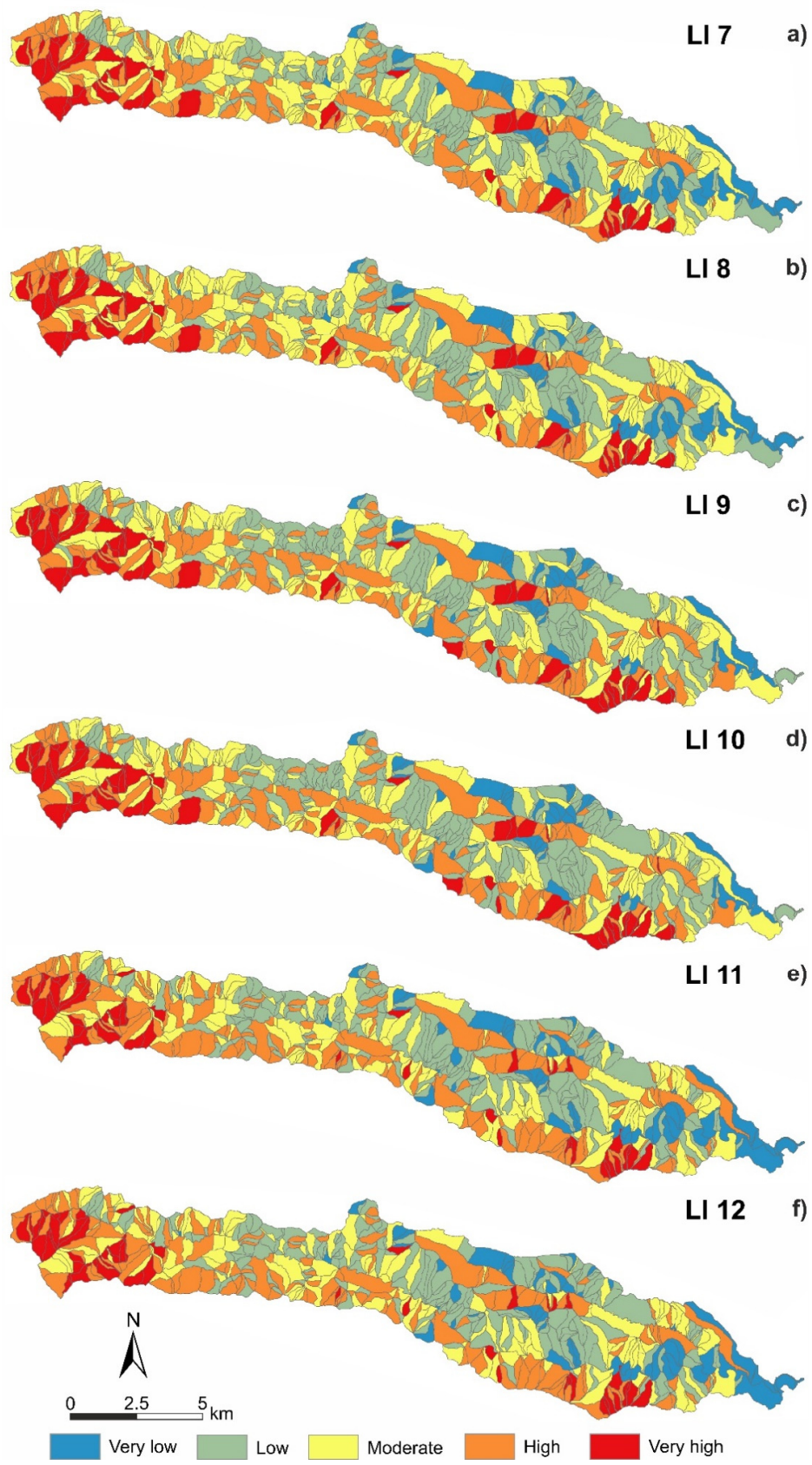

Figure 10. Landslide susceptibility maps created with the LI method: (**a**) LI_7 model; (**b**) LI_8 model; (**c**) LI_9 model; (**d**) LI_10 model; (**e**) LI_11 model; (**f**) LI_12 model.

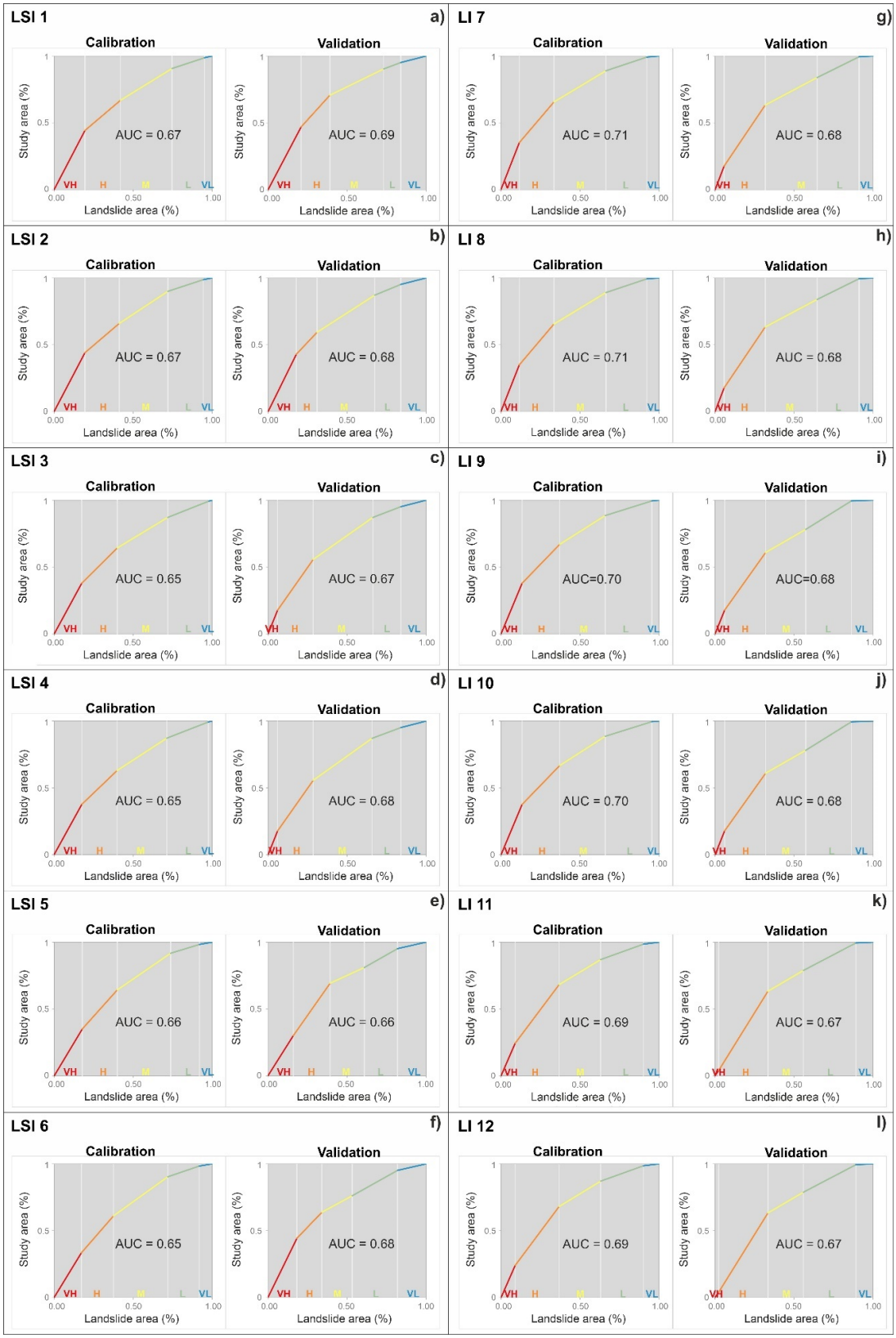

Figure 11. ROC curves with AUC values for the calibration and validation procedures (x-axis, percentage of the cumulative landslides area in each susceptibility classes; y-axis, percentage of the cumulative study area in each susceptibility classes) of the different models: (**a**) LSI_1 model; (**b**) LSI_2 model; (**c**) LSI_3 model; (**d**) LSI_4 model; (**e**) LSI_5 model; (**f**) LSI_6 model (**g**) LI_7 model; (**h**) LI_8 model; (**i**) LI_9 model; (**j**) LI_10 model; (**k**) LI_11 model; (**l**) LI_12 model.

The AUC values of the LI models were between 0.69 and 0.71. Therefore, the training accuracies were between 69% and 70%. The AUC values of the validation set were between 0.67 and 0.68, reaching a prediction accuracy between 67% and 68%. Almost all LI models reached the minimum threshold of the AUC value for reliability, with values around 0.7 [58]. The LI models with the highest AUC values were LI_7 and LI_8, which considered all the parameters, with and without the areal threshold of landslides.

In general, the LI models reached the highest validity, with the best performance for models LI_7 and LI_8. Concerning the different combinations of predisposing factors, the models with higher validity were those that considered all the parameters, while the areal threshold of landslides had no influence.

4. Discussion

In this study, we applied the LS method in a given study area (Piomba basin, Central Italy), providing a simple and straightforward way to statistically analyze the propensity for landslide based on the distribution of the predisposing factors. A multidisciplinary approach was applied that combined LiDAR-derived DTM analysis, aerial photo interpretation, GIS processing, past geomorphological maps analysis, and direct field surveys. This approach allowed us to obtain an up-to-date and reliable landslide inventory map and to select the predisposing factors with the appropriate accuracy and resolution. The use of remote sensing data provided us the possibility to validate the field survey in order to obtain ground-truth maps; moreover, the comparison of the present (field) with the past (aerial photos and DTM) terrain features highlighted the main changes in the terrain, allowing us to more efficiently detect and delimit the landforms.

The study area was segmented into SUs by developing an original GIS-based procedure starting from the terrain hydrography. The landslide index [15] approach via bivariate statistics was applied by adapting the grid-cell analysis to the vector analysis.

The outcomes of the statistical analyses can be summarized as follows:

- The two statistical methods applied (LSI and LI) can be used interchangeably because both of them describe the relative influence of each class of each factor;
- The method that reached higher statistical validity is the LI method (the simplified version of LSI), which resulted in a slightly higher value of AUC;
- With regards to the accuracy level, the models' performance is sufficient for only a few of the factors and is almost equivalent for the two statistical methods (LI and LSI);
- The best predictive models were LI_7 and LI_8 (created with the LI statistical method considering all the parameters with and without the areal threshold of landslides, respectively), reaching a prediction accuracy of 71%;
- The results of the different models are substantially in agreement when detecting the factor classes that have primary importance for the development of landslides in the study area: the landslides are mainly located on slopes characterized by alternating sand and clay, occupied by broad-leaved forests, with NW aspect, gradient between 15° and 20°, MSI values greater than 400 m, and low D (between 0.0001 and 1.2 km^{-1});
- The only significant difference observed between the two methods is the distribution of susceptibility classes in the study area; in particular, the very high susceptibility class characterizes a greater number of SUs in LSI maps than in LI maps;
- The LS models created by considering the complete landslide inventory do not differ from those that consider the landslides with an areal threshold of 2%, probably because there are few landslides under the threshold of 2% and these landslides do not affect the results;
- There are no differences between the models created by considering six factors (alternatively with S or MSI) rather than seven, indicating that MSI is effective in representing the morphometric characteristics of the SU: it includes a more effective quantification of the slope features related to the geomorphological processes distribution on the SUs; S characterizes the SUs only through the value of the gradient (in degrees), while MSI

includes a set of morphometric parameters such as slope, shape, and size. This result confirms previous studies on the validity of MSI as morphometric factor, e.g., [50].

From a statistical point of view, no further information is needed to explain the results. However, this distribution can be better understood if the relationships between landslides and predisposing factors are analyzed in detail from a geological and geomorphological point of view. Some general considerations can be extrapolated from the local level (i.e., study case) focusing on the geomorphological implication of the statistical results.

Considering the morphometrical setting, the most influential classes of S were found in general to be above 11°, with a slight predominance of the 16–20° class. This indicates that intermediate and high slope gradients (>11°) can lead to the formation of landslides in the study area, and few landslides form on low gradient hillslopes (<11°). The most influential class of MSI has an MSI value >400 m, with secondary classes of 230–300 m and 301–400 m. For SUs with an equal slope gradient, these classes correspond to longer and wider hillslopes, which hold most of the landslide area. Generally, longer hillslopes are also wider, which can induce the formation of flow-type and rotational landslides on soft clay–sand bedrock, such as the Apennine hills [16,60]. The effect is directly controlled by the water infiltration capacity and terrain saturation associated with the specific hydrogeological and lithological setting. The presence of local aquifers in sand sequences confined by undelaying clay deposits [16] and the subsequent high values of neutral pressure can result in increasing flow-type landslides [61].

The slope gradient values are connected to the geo-lithological context of the study area, which is mainly constituted by soft lithologies (clay, and alternating sand and clay). In the study area, low-gradient (i.e., $\leq$10°) SUs correspond to alluvial deposits, while medium-high-gradient (i.e., >11°) SUs correspond almost equally to the clay, alternating sand and clay, and sandstone/conglomerate layers. The presence of thick layers of sands within the clay can allow the slope to have a higher slope gradient. Moreover, the slope can be linked to the thickness of slope deposits derived from a linear relation with the local slope [45]: T is higher when S is lower [43].

The drainage density is different within the SUs: in many SUs, the value of D is 0 km^{-1}, indicating the absence of streams within the SUs; a number of SUs have a D value >5 km^{-1}; and most of the SUs have D values in classes ranging from 0.0001 to 5 km^{-1}. The primary influential class was that with lower D values (0.0001–1.2 km^{-1}), but all the classes with a D value <5 km^{-1} had almost the same probability of being affected by landslides. Therefore, there is no distinctive class of D that influences the landslide proneness in the study area. This outcome can again be linked to the geo-lithological setting: in an area with a quite uniform distribution of lithological units (mainly constitutes by soft lithologies), the distribution of D is also uniform and reflects the landslide proneness in relation to the landslide types (flows and rotational).

Considering the LULC factor, it is homogeneous and poorly differentiated in the study area; therefore, its effect can only be local. The most influential class was found to be the broad-leaved forests. This is related to the fact that they occur only on small portions of the basin, mainly located in the upstream area. Almost all the SUs with this prevalence are affected by landslides. The secondary LULC class was found to be olive groves; in this case, the landslide clusters in the SUs also fall within this type of cultivation. The territory is principally occupied by sparsely vegetated areas, complex cultivation, and land principally occupied by agriculture, with significant areas of natural vegetation, which were found to have a low impact on the occurrence of landslides. However, in these areas, the superficial evidence of landslides can be modified by human intervention, especially by agricultural practices, which, in many cases, can temporarily obliterate the landforms [16]. Moreover, the construction and the maintenance of the country roads in some cases can affect the predisposition of a slope to small landslides or, vice versa, on the obliteration of the superficial signs of the landslides.

Regarding the slope aspect, the most relevant orientation was found to be NW, and secondarily NE and N. This parameter has often been correlated with the effect of thermal

excursions and the more humid and wet condition of clayey sediments and superficial colluvial deposits with respect to the southern-facing hillslopes affected by wet/dry cycles [46]. However, in our case, the link between landslide distribution and slope aspect is more probably connected to the local bedrock structural setting, as already mentioned in previous studies [46,47]. In particular, in the main (homoclinal) valley, the cuesta structure caused the north-facing slopes (N, NE, and NW) to have a dip direction and the south-facing slopes (S, SE and SW) to have an anti-dip direction, while in the secondary (cataclinal) valleys, the E-facing and the S-facing slopes show a cross-dip direction. Generally, dip slopes have a greater propensity for landslides, while anti-dip slopes have greater stability. In this case study, the slope aspect can be considered an indirect factor of bedrock local geological structure [46].

Considering the other geomorphological processes that occur in the study area and that were included in the Geomorphological Map (Figure 3), some interesting considerations can be noted. In many cases, the SUs with a higher MSI and S (and subsequently lower T) correspond to the side slopes of badland basins. In general, they have a steep and rough morphology (which is quantified by high MSI values). This is due to the badland erosion process (i.e., linear incision inside the main gullies) [18,23,62] over drainage basins and slopes with a dense hydrographic network, and is favored by the lithology, in which the presence of thick layers of sands within the clay can allow the conservation of a high slope gradient. This determines that the corresponding SUs have also high D values (e.g., >5): in these cases, the main geomorphological processes are linear erosion (rill erosion, gully erosion, and piping) with a secondary role of the very shallow landslides (i.e., mud flows), which tend to fill the main channel [19,54].

The predisposing factors that reached higher importance in the statistical analysis are not necessarily the most important in the general geomorphological analysis, and vice versa. This is the case for D and L if we consider the LSI models. In this specific study area, they are poorly statistically significant due to the homogeneity of the terrain features, indicating that the predisposing factors are spatially associated, and their importance is dependent on local terrain features. From a geomorphological perspective, the most important predisposing factors are the geolithological features (L), to which other parameters are related. The morphometrical (MSI and S), morphological (A), and hydrographic (D) parameters are directly linked to the lithology of the terrain, which in turn is indirectly linked to other geological characteristics, such as the geological structure.

5. Conclusions

The results of this research study, through the creation of an up-to-date and detailed geomorphological map of the Piomba Stream basin, led to the development of an LSM that shows the areas most prone to landslides. The work was based on a multidisciplinary approach that combined direct field surveys, past geomorphological maps, LiDAR-derived DTM analysis, digital orthophotos interpretation, and GIS processing. The use of remote sensing data and applications can allow the landslide susceptibility assessment to be improved, in particular for the landslide inventory's creation and the predisposing factors, ensuring the ground truth of the field-based mapping.

Two statistical GIS-based bivariate statistical methods were applied based on the landslide index approach [15] through the simple transpositions of raster methods into vectors. An original and simple method for delineating the SUs was presented that is fully consistent with the physiography of the terrain and the conceptual image of the segmentation of the landscape into SUs [9,14]. Furthermore, the morphometric parameter MSI was successfully considered as a predisposing factor in LS analysis for the first time. The outcomes confirm the possibility of using MSI as the only morphometric factor in landslide susceptibility analysis, which was shown to be more representative of the slope's morphometry compared to S, especially in relation to the distribution of linear and areal erosion processes on the SUs.

The results of the statistics reached an adequate level of accuracy. An in-depth analysis and discussion of the results was conducted to link the outcomes of the statistical analysis to the geological and geomorphological features of the study area from a geomorphological point-of-view. The relationships between the predisposing factors and their consistency with the morphodynamic models were highlighted: the predisposing factors are strictly related with each other and with the local terrain features. We confirm that the geo-lithological factors are the main drivers for landslides in the study area, whether we consider them directly or indirectly as variables of the statistical models [3,4]. The predisposing factors used in the landslide susceptibility model of the Piomba Stream basin are spatially associated [4,58], and their importance is strictly dependent on local terrain characteristics [23,63]. These considerations can be extended to other basins of the Periadriatic foothills area, which has similar characteristics in terms of geological and geomorphological features.

This study highlighted the importance of examining the outcomes of the statistical analysis in a geomorphological perspective. The most important variable in the models is the lithology, which is directly related to the morphometry (MSI and S), morphology (A), and the hydrography (D) of the terrain and indirectly related the geological structure. However, some parameters play a priority role in the statistical analysis but a secondary role if we consider their geomorphological importance, and vice versa. This is the case with D and L, mainly due to the local conditions related to the homogeneity of the terrain features in the study area.

The observed similar statistical relevance values confirmed that both the LS methods (LI and LSI) have similar predictive skills [58] and can be used interchangeably. They provide quantitative indications, supported by geomorphological observations, of the propensity to landslide, reaching an adequate validation level. They must be further expanded and investigated, but surely can be useful if associated with some geomorphological considerations, in particular concerning the influence of one parameter on the others and the local terrain characteristics. The approach used in this study may be applied to similar morpho-geo-climatic areas and contexts, such as the Adriatic hilly area, as confirmed by previous work [45].

Author Contributions: Conceptualization, L.C. and M.B.; methodology, L.C. and D.M.; validation, L.C. and D.M.; formal analysis, L.C. and D.M.; investigation, D.M.; resources, L.C.; data curation, L.C.; writing—original draft preparation, L.C. and T.P.; writing—review and editing, L.C.; supervision, M.B.; project administration, M.B. All authors have read and agreed to the published version of the manuscript.

Funding: This research received funding from Università degli Studi "G. d'Annunzio" Chieti-Pescara (University fund ex60% 2018 M. Buccolini).

Institutional Review Board Statement: Not applicable.

Informed Consent Statement: Not applicable.

Data Availability Statement: Data will be available upon request.

Acknowledgments: The topographic data used for the geomorphological analysis were provided by the Struttura Speciale di Supporto Sistema Informativo Regione Abruzzo (http://www.regione.abruzzo.it/xcartografia/; http://opendata.regione.abruzzo.it/catalog, accessed on 1 September 2019). The authors would like to thank the Editor and the two anonymous reviewers whose revisions improved the quality of the manuscript.

Conflicts of Interest: The authors declare no conflict of interest.

Appendix A

Table A1. Values of the parameters for deriving the LSI for the models LSI_1–LSI_3–LSI_5.

LSI Method—All the Landslides (LSI_1–LSI_3–LSI_5)						
Factor ID	**Class**	**a**	**b**	**LI**	**LI_{nor}**	**Area_SU (km^2)**
	Bedrock					
1	Fluvial deposit	0.005	0.066	0.068	2.942	4.867
2	Sandstone and conglomerate	0.037	0.042	0.876	37.761	3.504
3	Clay	0.833	0.838	0.995	42.855	71.821
4	Alternating sand and clay	0.126	0.054	2.321	100	5.6
	Aspect					
1	N	0.036	0.024	1.489	65.199	2.206
2	NE	0.322	0.196	1.643	71.953	18.487
3	E	0.119	0.137	0.870	38.099	11.492
4	SE	0.110	0.134	0.817	35.786	11.186
5	SE	0.067	0.178	0.375	16.409	13.801
6	SW	0.022	0.075	0.297	13.008	5.759
7	W	0.086	0.151	0.570	24.967	12.096
8	NW	0.239	0.104	2.284	100	10.763
	Land cover and land use					
1	Non-irrigated arable land	0.159	0.331	0.480	12.343	26.079
2	Vineyards	0.001	0.010	0.078	2.008	0.707
3	Olive groves	0.083	0.033	2.480	63.746	3.535
4	Annual crops associated with permanent crop	0.020	0.063	0.317	8.154	4.806
5	Complex cultivation	0.433	0.280	1.550	39.830	26.062
6	Land principally occupied by agriculture	0.130	0.167	0.776	19.944	13.841
7	Broad-leaved forest	0.159	0.041	3.891	100	5.105
8	Transitional woodland shrub	0.006	0.014	0.452	11.610	1.102
9	Sparsely vegetated areas	0.008	0.061	0.138	3.554	4.554
	Drainage density (km^{-1})					
1	0	0.405	0.401	1.009	94.760	34.467
2	0.0001–1.2	0.211	0.199	1.065	100	17.207
3	1.2–2.5	0.208	0.198	1.048	98.473	17.154
4	2.5–5	0.165	0.169	0.977	91.775	14.476
5	>5	0.010	0.032	0.318	29.895	2.487
MSI						
1	11–35	0.017	0.016	1.042	46.494	1.406
2	36–50	0.036	0.033	1.107	49.389	2.865
3	51–90	0.108	0.188	0.574	25.608	15.071
4	91–170	0.253	0.333	0.758	33.821	27.520
5	171–230	0.157	0.147	1.072	47.852	12.736
6	231–300	0.142	0.108	1.320	58.914	9.714
7	301–400	0.110	0.096	1.148	51.214	8.429
8	>400	0.176	0.079	2.241	100	8.049
	Slope (°)					
1	0–10	0.015	0.102	0.147	11.832	7.616
2	11–15	0.279	0.272	1.026	82.824	23.418
3	16–20	0.450	0.364	1.239	100	32.351
4	>20	0.256	0.262	0.975	78.729	22.405
	Deposits thickness (m)					
1	0–2	0.002	0.006	0.259	25.832	0.486
2	>3	0.995	0.994	1.001	100	85.260

Table A2. Factors' weights for the models LSI_1–LSI_3–LSI_5.

LSI Method—All the Landslides (LSI_1–LSI_3–LSI_5)			
Factor	**w (6 Factors)**	**w (5 Factors)**	**w (5 Factors)**
Bedrock	0.026	0.030	0.034
Aspect	0.117	0.131	0.152
Land cover and land use	0.018	0.020	0.023
Drainage density	0.269	0.301	0.350
MSI	0.230	0.258	/
Slope	0.106	/	0.138
Deposits thickness	0.232	0.260	0.302

Table A3. Values of the parameters for deriving the LSI for the models LSI_2–LSI_4–LSI_6.

LSI Method—Landslides Area > 2% (LSI_2–LSI_4–LSI_6)						
Factor ID	**Class**	**a**	**b**	**LI_1**	**LI_{1nor}**	**Area_SU (km)**
	Bedrock					
1	Fluvial deposit	0.005	0.066	0.069	2.878	4.867
2	Sandstone and conglomerate	0.036	0.042	0.862	35.961	3.504
3	Clay	0.830	0.838	0.990	41.331	71.821
4	Alternating sand and clay	0.129	0.054	2.396	100	5.6
	Aspect					
1	N	0.036	0.024	1.489	65.199	2.206
2	NE	0.322	0.196	1.643	71.953	18.487
3	E	0.119	0.137	0.870	38.099	11.492
4	SE	0.110	0.134	0.817	35.786	11.186
5	S	0.067	0.178	0.375	16.409	13.801
6	SW	0.022	0.075	0.297	13.008	5.759
7	W	0.086	0.151	0.570	24.967	12.096
8	NW	0.239	0.104	2.284	100	10.763
	Land cover and use					
1	Non-irrigated arable land	0.159	0.331	0.480	12.343	26.079
2	Vineyards	0.001	0.010	0.078	2.008	0.707
3	Olive groves	0.083	0.033	2.480	63.746	3.535
4	Annual crops associated with permanent crop	0.020	0.063	0.317	8.154	4.806
5	Complex cultivation	0.433	0.280	1.550	39.830	26.062
6	Land principally occupied by agriculture	0.130	0.167	0.776	19.944	13.841
7	Broad-leaved forest	0.159	0.041	3.891	100	5.105
8	Transitional woodland shrub	0.006	0.014	0.452	11.610	1.102
9	Sparsely vegetated areas	0.008	0.061	0.138	3.554	4.554
	Drainage density (km^{-1})					
1	0	0.405	0.401	1.009	94.760	34.467
2	0.0001–1.2	0.211	0.199	1.065	100	17.207
3	1.2–2.5	0.208	0.198	1.048	98.473	17.154
4	2.5–5	0.165	0.169	0.977	91.775	14.476
5	>5	0.010	0.032	0.318	29.895	2.487
MSI						
1	11–35	0.017	0.016	1.042	46.494	1.406
2	36–50	0.036	0.033	1.107	49.389	2.865
3	51–90	0.108	0.188	0.574	25.608	15.071
4	91–170	0.253	0.333	0.758	33.821	27.520
5	171–230	0.157	0.147	1.072	47.852	12.736
6	231–300	0.142	0.108	1.320	58.914	9.714
7	301–400	0.110	0.096	1.148	51.214	8.429
8	>400	0.176	0.079	2.241	100	8.049
	Slope (°)					
1	0–10	0.015	0.1025	0.146	11.832	7.616
2	11–15	0.279	0.2719	1.026	82.824	23.418
3	16–20	0.450	0.3635	1.239	100	32.351
4	>20	0.256	0.2622	0.975	78.729	22.405
	Deposits thickness (m)					
1	0–2	0.001	0.007	0.200	23.590	0.503
2	>3	0.256	0.2622	0.975	78.729	85.242

Table A4. Factors' weight for the models LSI_2–LSI_4–LSI_6.

	LSI Method—Landslides Area > 2% (LSI_2–LSI_4–LSI_6)		
Factord	**w (6 Factors)**	**w (5 Factors)**	**w (5 Factors)**
Bedrock	0.026	0.030	0.035
Aspect	0.120	0.136	0.159
Land cover and use	0.019	0.021	0.025
Drainage density	0.260	0.292	0.343
MSI	0.244	0.274	/
Slope	0.112	/	0.148
Deposits thickness	0.220	0.247	0.290

Table A5. Values of the parameters for deriving the LI for the models LI_7–LI_9–LI_11.

	LI Method—All the Landslides (LI_7–LI_9–LI_11)			
Factor ID	**Class**	**LI_2**	**LI_{2nor}**	**Area_SU (km)**
	Bedrock			
1	Fluvial deposit	0.013	4.183	4.867
2	Sandstone and conglomerate	0.140	46.768	3.504
3	Clay	0.156	52.169	71.821
4	Alternating sand and clay	0.299	100	5.6
	Aspect			
1	N	0.216	72.597	2.206
2	NE	0.234	78.523	18.487
3	E	0.139	46.613	11.492
4	SE	0.132	44.156	11.186
5	S	0.065	21.800	13.801
6	SW	0.052	17.517	5.759
7	W	0.096	32.083	12.096
8	NW	0.298	100	10.763
	Land cover and use			
1	Non-irrigated arable land	0.082	19.548	26.079
2	Vineyards	0.014	3.407	0.707
3	Olive groves	0.315	75.165	3.535
4	Annual crops associated with permanent crop	0.056	13.255	4.806
5	Complex cultivation	0.223	53.273	26.062
6	Land principally occupied by agriculture	0.126	30.012	13.841
7	Broad-leaved forest	0.419	100	5.105
8	Transitional woodland shrub	0.077	18.440	1.102
9	Sparsely vegetated areas	0.025	5.964	4.554
	Drainage density (km^{-1})			
1	0	0.158	95.726	34.467
2	0.0001–1.2	0.165	100	17.207
3	1.2–2.5	0.163	98.723	17.154
4	2.5–5	0.162	97.994	14.476
5	>5	0.052	31.607	2.487
MSI				
1	11–35	0.162	55.155	1.406
2	36–50	0.170	58.005	2.865
3	51–90	0.096	32.761	15.071
4	91–170	0.123	42.003	27.501
5	171–230	0.166	56.669	12.698
6	231–300	0.197	66.992	9.714
7	301–400	0.175	59.773	8.429
8	>400	0.294	100	8.049
	Slope (°)			
1	0–10	0.026	14.157	7.616
2	11–15	0.160	85.657	23.418
3	16–20	0.187	100	32.351
4	>20	0.153	81.938	22.405
	Deposits thickness (m)			
1	0–2	0.045	29.22	0.486
2	>3	0.157	100	85.247

Table A6. Values of the parameters for deriving the LI for the models LI_8–LI_10–LI_12.

LI Method—Landslides Area > 2% (LI_8–LI_10–LI_12)				
Factor ID	**Class**	**LI_2**	**LI_{2nor}**	**Area_SU (km)**
	Bedrock			
1	Fluvial deposit	0.012	4.090	4.867
2	Sandstone and conglomerate	0.136	44.695	3.504
3	Clay	0.154	50.385	71.725
4	Alternating sand and clay	0.305	100	5.637
	Aspect			
1	N	0.216	72.755	2.206
2	NE	0.230	77.271	18.449
3	E	0.137	46.200	11.492
4	SE	0.131	43.969	11.186
5	S	0.065	21.763	13.801
6	SW	0.052	17.420	5.759
7	W	0.095	31.784	12.096
8	NW	0.297	100	10.744
	Land cover and use			
1	Non-irrigated arable land	0.082	19.509	26.028
2	Vineyards	0.014	3.407	0.707
3	Olive groves	0.292	69.657	3.535
4	Annual crops associated with permanent crop	0.055	13.016	4.806
5	Complex cultivation	0.223	53.198	26.055
6	Land principally occupied by agriculture	0.125	29.735	13.841
7	Broad-leaved forest	0.419	100	5.105
8	Transitional woodland shrub	0.077	18.431	1.102
9	Sparsely vegetated areas	0.021	5.096	4.554
	Drainage density (km^{-1})			
1	0	0.157	96.037	34.416
2	0.0001–1.2	0.164	100	17.207
3	1.2–2.5	0.162	99.025	17.154
4	2.5–5	0.155	94.873	13.743
5	>5	0.048	29.537	2.660
MSI				
1	11–35	0.162	56.628	1.406
2	36–50	0.170	59.534	2.865
3	51–90	0.095	33.201	15.071
4	91–170	0.122	42.759	27.501
5	171–230	0.165	57.854	12.698
6	231–300	0.196	68.629	9.714
7	301–400	0.175	61.116	8.429
8	>400	0.286	100	8.049
	Slope (°)			
1	0–10	0.026	14.317	7.616
2	11–15	0.159	86.242	23.380
3	16–20	0.184	100	32.331
4	>20	0.152	82.304	22.405
	Deposits thickness (m)			
1	0–2	0.037	23.59	0.486
2	>3	0.157	100	85.247

Table A7. Thresholds between the susceptibility classes for the models created with the LSI method.

	LSI_1	**LSI_2**	**LSI_3**	**LSI_4**	**LSI_5**	**LSI_6**
Very low	0.00–60.67	0.00–59.96	0.00–54.98	0.00–56.01	0.00–69.69	0.00–68.08
Low	60.68–70.33	59.97–69.55	54.99–69.33	56.00–68.10	70.00–80.72	68.09–79.90
Moderate	70.34–75.25	69.56–74.74	69.34–74.77	68.11–73.74	80.73–85.45	79.91–84.85
High	75.26–81.38	74.75–81.07	74.78–81.50	73.75–80.68	85.46–90.82	84.86–90.49
Very high	81.39–100	81.08–100	81.51–96.63	80.69–100	90.83–100	90.50–100

Table A8. Thresholds between the susceptibility classes for the models created with the LI method.

	LI7	LI8	LI9	LI10	LI11	LI12
Very low	0.00–54.31	0.00–54.32	0.00–50.21	0.00- 50.21	0.00–56.16	0.00–56.16
Low	54.32–64.24	54.33–64.14	50.22–60.11	50.22–60.11	56.17–67.39	56.17–67.39
Moderate	64.25–70.96	64.15–70.95	60.12–67.37	60.12–67.37	67.40–73.68	67.40–73.68
High	70.97–78.73	70.96–78.73	67.38–75.19	67.38–75.19	73.69–82.19	73.69–82.19
Very high	78.74–100	78.74–100	75.20–100	75.20–100	82.20–100	82.20–100

References

1. Brabb, E.E. Innovative approaches to landslide hazard and risk mapping. In *Proceedings 4th International Symposium on Landslides*; Canadian Geotechnical Society: Toronto, ON, Canada, 1984; pp. 307–324. [CrossRef]
2. Fell, R.; Corominas, J.; Bonnard, C.; Cascini, L.; Leroi, E.; Savage, W.Z. Guidelines for landslide susceptibility, hazard and risk zoning for land-use planning. *Eng. Geol.* **2008**, *102*, 85–98. [CrossRef]
3. Reichenbach, P.; Rossi, M.; Malamud, B.D.; Mihir, M.; Guzzetti, F. A review of statistically-based landslide susceptibility models. *Earth-Sci. Rev.* **2018**, *180*, 60–91. [CrossRef]
4. Guzzetti, F.; Carrara, A.; Cardinali, M.; Reichenbach, P. Landslide hazard evaluation: A review of current techniques and their application in a multi-scale study, Central Italy. *Geomorphology* **1999**, *31*, 181–216. [CrossRef]
5. Guzzetti, F.; Reichenbach, P.; Ardizzone, F.; Cardinali, M.; Galli, M. Estimating the quality of landslide susceptibility models. *Geomorphology* **2006**, *81*, 166–184. [CrossRef]
6. Van Westen, C.J.; Van Asch, T.W.J.; Soeters, R. Landslide hazard and risk zonation: Why is it still so difficult? *Bull. Eng. Geol. Environ.* **2006**, *65*, 167–184. [CrossRef]
7. Carrara, A.; Cardinali, M.; Guzzetti, F.; Reichenbach, P. GIS technology in mapping landslide hazard. In *Geographical Information Systems in Assessing Natural Hazards*; Carrara, A., Guzzetti, F., Eds.; Kluwer: Dordrecht, The Netherlands, 1995; pp. 35–176. [CrossRef]
8. Rotigliano, E.; Cappadonia, C.; Conoscenti, C.; Costanzo, D.; Agnesi, V. Slope units-based flow susceptibility model: Using validation tests to select controlling factors. *Nat. Hazards* **2012**, *61*, 143–153. [CrossRef]
9. Amato, G.; Eisank, C.; Castro-Camilo, D.; Lombardo, L. Accounting for covariate distributions in slope unit-based landslide susceptibility models. A case study in the alpine environment. *Eng. Geol.* **2019**, *260*, 1–13. [CrossRef]
10. Alvioli, M.; Marchesini, M.; Reichenbach, P.; Rossi, M.; Ardizzone, F.; Fiorucci, F.; Guzzetti, F. Automatic delineation of geomorphological slope units with r.slopeunits v1.0 and their optimization for landslide susceptibility modelling. *Geosci. Model Dev.* **2016**, *9*, 3975–3991. [CrossRef]
11. Van Den Eeckhaut, M.; Reichenbach, P.; Guzzetti, F.; Rossi, M.; Poesen, J.A. Combined landslide inventory and susceptibility assessment based on different mapping units: An example from the Flemish Ardennes, Belgium. *Nat. Hazards Earth Syst. Sci.* **2009**, *9*, 507–521. [CrossRef]
12. Ba, Q.; Chen, Y.; Deng, S.; Yang, J.; Li, H. A comparison of slope units and grid cells as mapping units for landslide susceptibility assessment. *Earth Sci. Inform.* **2018**, *11*, 373–388. [CrossRef]
13. Jacobs, L.; Kervyn, M.; Reichenbach, P.; Rossi, M.; Marchesini, I.; Alvioli, M.; Dewitte, O. Regional susceptibility assessments with heterogeneous landslide information: Slope unit- vs. pixel-based approach. *Geomorphology* **2020**, *356*, 1–12. [CrossRef]
14. Martinello, C.; Cappadonia, C.; Conoscenti, C.; Agnesi, V.; Rotigliano, E. Optimal slope units partitioning in landslide susceptibility mapping. *J. Maps* **2020**, 1–11. [CrossRef]
15. Van Westen, C.J.; Rengers, N.; Terlien, M.T.J.; Soeters, R. Prediction of the occurrence of slope instability phenomena through GIS based hazard zonation. *Geol. Rundsch* **1997**, *86*, 404–414. [CrossRef]
16. Buccolini, M.; Gentili, B.; Materazzi, M.; Aringoli, D.; Pambianchi, G.; Piacentini, T. Human impact and slope dynamics evolutionary trends in the monoclinal relief of the Adriatic central Italy. *Catena* **2007**, *71*, 96–109. [CrossRef]
17. Buccolini, M.; Gentili, B.; Materazzi, M.; Piacentini, T. Late Quaternary geomorphological evolution and erosion rates in the clayey peri-Adriatic belt (central Italy). *Geomorphology* **2010**, *116*, 145–161. [CrossRef]
18. Buccolini, M.; Coco, L. The role of the hillside in determining the morphometric characteristics of calanchi: The example of Adriatic Central Italy. *Geomorphology* **2010**, *123*, 200–210. [CrossRef]
19. Buccolini, M.; Coco, L. MSI (morphometric slope index) for analyzing activation and evolution of calanchi in Italy. *Geomorphology* **2013**, *191*, 142–149. [CrossRef]
20. Piacentini, T.; Galli, A.; Marsala, V.; Miccadei, E. Analysis of Soil Erosion Induced by Heavy Rainfall: A Case Study from the NE Abruzzo Hills Area in Central Italy. *Water* **2018**, *10*, 1314. [CrossRef]
21. Vessia, G.; Di Curzio, D.; Chiaudani, A.; Rusi, S. Regional rainfall threshold maps drawn through multivariate geostatistical techniques for shallow landslide hazard zonation. *Sci. Total Environ.* **2020**, *705*, 135815. [CrossRef]
22. Costanzo, D.; Rotigliano, E.; Irigaray, C.; Jiménez-Perálvarez, J.D.; Chacón, J. Factors selection in landslide susceptibility modelling on large scale following the GIS matrix method: Application to the River Beiro Basin (Spain). *Nat. Hazards Earth Syst. Sci.* **2012**, *12*, 327–340. [CrossRef]

23. Pourghasemi, H.R.; Rahmadi, O. Prediction of the landslide susceptibility: Which algorithm, which precision? *Catena* **2018**, *162*, 177–192. [CrossRef]
24. Buccolini, M.; Coco, L.; Cappadonia, C.; Rotigliano, E. Relationships between a new slope morphometric index and calanchi erosion in northern Sicily, Italy. *Geomorphology* **2012**, *149–150*, 41–48. [CrossRef]
25. Fazzini, M.; Giuffrida, A. Une nouvelle proposition quantitative des régimes pluviométriques dans le territoire de Italie: Premiers résultats. In *Climat Urbain, Ville et Architecture*; Acts XVIII Colloque Internationale de Climatologie: Genova, Italy, 2005; pp. 361–365.
26. Buccolini, M.; Bufalini, M.; Coco, L.; Materazzi, M.; Piacentini, T. Small catchments evolution on clayey hilly landscapes in Central Apennines and northern Sicily (Italy) since the Late Pleistocene. *Geomorphology* **2020**, *363*, 1–19. [CrossRef]
27. Cantalamessa, G.; Di Celma, C. Sequence response to syndepositional regional uplift: Insights from high-resolution sequence stratigraphy of late Early Pleistocene strata, Periadriatic Basin, Central Italy. *Sediment. Geol.* **2004**, *164*, 283–309. [CrossRef]
28. Crescenti, U.; Milia, M.L.; Rusciadelli, G. Stratigraphic and tectonic evolution of the Pliocene Abruzzi basin (Central Apennines, Italy). *Boll. Della Soc. Geol. Ital.* **2004**, *123*, 163–173. [CrossRef]
29. Bigi, S.; Conti, A.; Casero, P.; Ruggiero, L.; Recanati, R.; Lipparini, L. Geological model of the central Periadriatic basin (Apennines, Italy). *Mar. Pet. Geol.* **2013**, *42*, 107–121. [CrossRef]
30. D'Alessandro, L.; Miccadei, E.; Piacentini, T. Morphotectonic study of the lower Sangro River valley (Abruzzi, Central Italy). *Geomorphology* **2008**, *102*, 145–158. [CrossRef]
31. Abruzzo-Sangro Basin Authority (2005) Piano Stralcio di Bacino per l'Assetto Idrogeologico dei Bacini di Rilievo Regionale Abruzzesi e del Bacino del Fiume Sangro. (L.R. 18.05 1989 n.81 e L. 24.08.2001)– Carta inventario– scala 1:25.000. Available online: http://autoritabacini.regione.abruzzo.it/index.php/carta-inventario-pai (accessed on 1 September 2019).
32. ISPRA (2007) IFFI, Inventario dei Fenomeni Franosi in Italia. Available online: http://www.apat.gov.it/site/it-IT/Progetti/IFFI_-_Inventario_dei_fenomeni_franosi_in_Italia/. (accessed on 1 September 2019).
33. Varnes, D.J. Slope movement types and processes. In *Landslides, Analysis and Control, Special Report*; Schuster, R.L., Krizek, R.J., Eds.; National Academy of Sciences: Washington, DC, USA, 1978; pp. 11–33.
34. Marsala, V.; Galli, A.; Paglia, G.; Miccadei, E. Landslide Susceptibility Assessment of Mauritius Island (Indian Ocean). *Geosciences* **2019**, *9*, 493. [CrossRef]
35. Guzzetti, F.; Cardinali, M.; Reichenbach, F. The Influence of Structural Setting and Lithology on Landslide Type and Pattern. *Env. Eng. Geosci.* **1996**, *2*, 531–555. [CrossRef]
36. Segoni, S.; Pappafico, G.; Luti, T.; Catani, F. Landslide susceptibility assessment in complex geological settings: Sensitivity to geological information and insights on its parameterization. *Landslides* **2020**, *17*, 2443–2453. [CrossRef]
37. Capolongo, D.; Pennetta, L.; Piccarreta, M.; Fallacara, G.; Boenzi, F. Spatial and temporal variations in soil erosion and deposition due to land-levelling in a semi-arid area of Basilicata (Southern Italy). *Earth Surf. Proc. Land.* **2008**, *33*, 364–379. [CrossRef]
38. Reichenbach, P.; Busca, C.; Mondini, A.C.; Rossi, M. The influence of land use change on landslide susceptibility zonation: The Briga catchment test site (Messina, Italy). *Environ. Manag.* **2014**, *54*, 1372–1384. [CrossRef] [PubMed]
39. Persichillo, M.G.; Bordoni, M.; Meisina, C. The role of land use changes in the distribution of shallow landslides. *Sci. Total Environ.* **2017**, *574*, 924–937. [CrossRef] [PubMed]
40. Corine Land Cover (2012) Land cover map. Environmental European Agency. Available online: http://land.copernicus.eu/ (accessed on 1 September 2019).
41. Dietrich, W.E.; Reiss, R.; Hsu, M.L.; Montgomery, D.R. A process based model for colluvial soil depth and shallow landsliding using digital elevation data. *Hydrol Process.* **1995**, *9*, 383–400. [CrossRef]
42. Lanni, C.; Mcdonnell, J.; Hopp, L.; Rigon, R. Simulated effect of soil depth and bedrock topography on near-surface hydrologic response and slope stability. *Earth Surf. Process. Landf.* **2013**, *38*, 146–159. [CrossRef]
43. Catani, F.; Segoni, S.; Falorni, G. An empirical geomorphology-based approach to the spatial prediction of soil thickness at catchment scale. *Water Resour. Res.* **2010**, *46*, 1–15. [CrossRef]
44. Pelletier, J.D.; Rasmussen, C. Geomorphically based predictive mapping of soil thickness in upland watersheds. *Water Resour. Res.* **2009**, *45*, 1–15. [CrossRef]
45. Sciarra, M.; Coco, L.; Urbano, T. Assessment and validation of GIS-based landslide susceptibility maps: A case study from Feltrino stream basin (Central Italy). *Bull. Eng. Geol. Env.* **2017**, *76*, 437–456. [CrossRef]
46. Capitani, M.; Ribolini, A.; Bini, M. The slope aspect: A predisposing factor for landsliding? *Comptes Rendus Geosci.* **2013**, *345*, 427–438. [CrossRef]
47. Fernandes, N.F.; Guimaranes, R.F.; Gomes, R.A.T.; Vieira, B.C.; Montgomery, D.R.; Greenberg, H. Topographic controls of landslides in Rio de Janeiro: Field evidence and modeling. *Catena* **2004**, *55*, 163–181. [CrossRef]
48. Horton, R.E. Erosional development of streams and their drainage basins: Hydrophysical approach to quantitative morphology. *Bull. Geol. Soc. Am.* **1945**, *56*, 275–375. [CrossRef]
49. Oguchi, T. Drainage density and relative relief in humid steep mountains with frequent slope failure. *Earth Surf. Process. Landf.* **1997**, *22*, 107–120. [CrossRef]
50. Tucker, G.; Bras, R.L. Hillslope processes, drainage density, and landscape morphology. *Water Resour. Res.* **1998**, *34*, 2751–2764. [CrossRef]

51. Istanbulluoglu, E.; Bras, R.L. Vegetation-modulated landscape evolution: Effects of vegetation on landscape processes, drainage density, and topography. *J. Geophys. Res.* **2005**, *110*, 1–19. [CrossRef]
52. Van Westen, C.J.; Rengers, N.; Soeters, R. Use of geomorphological information in indirect landslide susceptibility assessment. *Nat. Hazards* **2003**, *30*, 399–419. [CrossRef]
53. Yalcin, A.; Reis, S.; Aydinoglu, A.C.; Yomralioglu, T. A GIS-based comparative study of frequency ratio, analytical hierarchy process, bivariate statistics and logistics regression methods for landslide susceptibility mapping in Trabzon, NE Turkey. *Catena* **2011**, *85*, 274–287. [CrossRef]
54. Cappadonia, C.; Coco, L.; Buccolini, M.; Rotigliano, E. From slope morphometry to morphogenetic processes: An integrated approach of field survey, GIS morphometric analysis and statistics in Italian badlands. *Land Degrad. Dev.* **2016**, *27*, 851–862. [CrossRef]
55. Coco, L.; Buccolini, M. The morphometric slope index (MSI) as an indicator of landscape evolution: A multi-scale analysis. *Géomorphologie Relief Process. Environnement.* **2016**, *22*, 177–186. [CrossRef]
56. Romeo, R.W.; Mari, M.; Floris, M.; Pappafico, G.; Gori, U. An approach to join the spatial and temporal components of landslides susceptibility: An application to the Marche Region (Central Italy). *Ital. J. Eng. Geol. Env.* **2011**, *2*, 63–77. [CrossRef]
57. Lee, S.; Min, K. Statistical analysis of landslide susceptibility at Yongin, Korea. *Environ. Geol.* **2001**, *40*, 1095–1113. [CrossRef]
58. Steger, S.; Brenning, A.; Bell, R.; Petschko, H.; Glade, T. Exploring discrepancies between quantitative validation results and the geomorphic plausibility of statistical landslide susceptibility maps. *Geomorphology* **2016**, *262*, 8–23. [CrossRef]
59. Rossi, M.; Guzzetti, F.; Reichenbach, P.; Mondini, A.C.; Peruccacci, S. Optimal landslide susceptibility zonation based on multiple forecasts. *Geomorphology* **2010**, *114*, 129–142. [CrossRef]
60. Carabella, C.; Boccabella, F.; Buccolini, M.; Ferrante, F.; Pacione, P.; Gregori, C.; Pagliani, T.; Piacentini, T.; Miccadei, E. Geomorphology of landslide–flood-critical areas in hilly catchments and urban areas for EWS (Feltrino Stream and Lanciano town, Abruzzo, Central Italy). *J. Maps* **2021**, *17*, 40–53. [CrossRef]
61. Ahrendt, A.; Zuquette, L.V. Triggering factors of landslides in Campos do Jordao city, Brazil. *Bull. Eng. Geol. Environ.* **2003**, *62*, 231–234. [CrossRef]
62. Komac, M.A. landslide susceptibility model using the Analytical Hierarchy Process method and multivariate statistics in perialpine Slovenia. *Geomorphology* **2006**, *74*, 17–28. [CrossRef]
63. Lin, Y.P.; Chu, H.J.; Wu, C.F. Spatial pattern analysis of landslide using landscape metrics and logistic regression: A case study in Central Taiwan. *Hydrol. Earth Syst. Sci. Discuss.* **2010**, *7*, 3423–3451. [CrossRef]